CMS Analysis Note

The content of this note is intended for CMS internal use and distribution only

2011/12/02

Search for the standard model Higgs boson in the decay channel H $\rightarrow$ZZ$\rightarrow$ 2ℓ2b

L. Borrello[4], D. Bortoletto[4], R. Castello[5], G. Codispoti[6], A. De Cosa[3], D. Dominguez[2], F. Fabozzi[3], J. Fernandez de Troconiz[6], P. Garcia-Abia[2], O. Gonzalez[2], J. Hernandez[2], M. Kress[4], L. Lista[3], S. Meola[3], M. Narain[1], M. Segala[1], and M. Vidal[4]

[1] Brown University, Providence, RI, USA
[2] CIEMAT, Madrid, Spain
[3] INFN Sezioni di Napoli, Napoli, Italy
[4] Purdue University, West Lafayette, IN, USA
[5] UC Louvain, Belgium
[6] Universidad Autonoma de Madrid, Madrid, Spain

Abstract

We present a search for the standard model Higgs boson through its decay to two Z bosons, subsequently decaying to two leptons (electrons or muons) and two b-quark jets. The analysis exploits the kinematics of the final state, consisting on two leptons and two b-jets, to select the Higgs boson signal in the mass range from 200 GeV to 600 GeV. The full analysis is run using the whole amount of data collected by CMS in 2011.

Contents

1 Introduction

The Higgs boson is an essential element of the Standard Model (SM) of particles and their interactions explaining the origin of mass and playing a key role in the mechanism of electroweak symmetry breaking. Precision measurements of the W boson and top quark masses together with the Z pole variables constrain the mass of the Higgs boson which is a free parameter of the theory: currently the 95% one-sided confidence level upper limit on m_{H} is 158 GeV. Direct searches for the Higgs at LEP-II [1] set a 95% C.L. lower limit on m_{H} of 114.4 GeV, while the region between 158 GeV and 175 GeV has been excluded by the Tevatron experiments [2, 3]. The 95% C.L. upper limit on the Higgs mass increases from 158 GeV to 185 GeV when the results from the direct searches are included [4].

The CMS collaboration is performing searches for the Higgs in a several decay modes. This comprehensive effort aims at gaining sensitivity over a large range of Higgs masses by combining many different analyses. We expect that this effort will finally explore the region with $m_{\mathrm{H}} \geq 2m_{\mathrm{Z}}$ which is not probed at the Tevatron. In this note we report a detailed study of the prospect for the search for the Higgs boson in $\mathrm{H} \to \mathrm{ZZ}$ when one of Z decays as $\mathrm{Z} \to \ell^-\ell^+$ and the other as $\mathrm{Z} \to \mathrm{b\bar{b}}$. The dominant background is Z+jets production. Other minor backgrounds are $t\bar{t}$ and diboson production. The data and Monte Carlo sample used in this analysis are described in Section 2. The analysis strategy including the signal to background optimization are discussed in Sections 3 and 7. Contamination is estimated from background-enriched control samples. Methods to provide a data-driven derivation of the background is presented in Section 5. A detailed discussion of the systematic errors, including the impact of the pile-up events expected in the 2011 LHC run, as well as the modeling of the b-tagging algorithms in CMS, is described in Section 6. The strategy and the experimental methods are validated using X fb^{-1} data collected by the CMS experiment in 2011 as shown in Section 8.

2 Data and Monte Carlo samples

The data and Monte Carlo (MC) samples used in this analysis are described in this section. We are using 4 fb^{-1} of data collected in 2011. The MC samples, described in detail below, have been produced superimposing a number of minimum bias interactions to simulate the pile-up interactions in the event data. We are using the MC samples produced with the PU_S4 pile-up mixing scheme and the Summer11 reconstruction.

2.1 Background Monte Carlo

The dominant background in this analysis is the inclusive Z production together with jets, in particular with a pair of b-jets. We used the MADGRAPH generator [5] (table 1).

Name	σ LO(NLO) [pb]	Lumi LO(NLO) [fb^{-1}]
DYJetsToLL_TuneZ2_M-50_7TeV-madgraph-tauola	2289(3048)	15.85(11.90)

Table 1: Z+jets MC sample.

Other minor backgrounds are $t\bar{t}$ and diboson ZZ, WW, and WZ production. The samples used are listed in Table 2.

2.2 Signal Monte Carlo

The signal MC samples used in this analysis are summarized in Table 3. The POWHEG generator [6–8] was used. Only samples with the gluon fusion production mechanism are considered

Name	σ LO(NLO) [pb]	Lumi LO(NLO) [fb^{-1}]
TTTo2L2Nu2B_7TeV-powheg-pythia6	15.86(16.7)	651.92(619.12)
TTJets_TuneZ2_7TeV-madgraph-tauola	94(157.5)	39.38(23.50)
WW_TuneZ2_7TeV_pythia6_tauola	27.8(42.9)	152.01(98.51)
WZ_TuneZ2_7TeV_pythia6_tauola	10.4(18.3)	410.12(233.07)
ZZ_TuneZ2_7TeV_pythia6_tauola	4.30(5.9)	973.93(709.81)

Table 2: $t\bar{t}$, ZZ, WW, and WZ MC samples.

since the weak boson fusion production mechanism represents a small contribution and the kinematics is very similar. The total Higgs production cross-section which combines all production mechanisms is used for normalization.

Sample	$\sigma \times \mathrm{BR}_{ZZ} \times \mathrm{BR}_{2l2j}$ at NLO [fb]	Lumi [fb^{-1}]
GluGluToHToZZTo2L2Q_M-130_7TeV-powheg-pythia6	86.31	3436.46
GluGluToHToZZTo2L2Q_M-150_7TeV-powheg-pythia6	133.57	2143.72
GluGluToHToZZTo2L2Q_M-190_7TeV-powheg-pythia6	194.04	1467.40
GluGluToHToZZTo2L2Q_M-200_7TeV-powheg-pythia6	211.51	1346.25
GluGluToHToZZTo2L2Q_M-210_7TeV-powheg-pythia6	205.02	1384.06
GluGluToHToZZTo2L2Q_M-220_7TeV-powheg-pythia6	193.30	1451.42
GluGluToHToZZTo2L2Q_M-230_7TeV-powheg-pythia6	179.56	1621.86
GluGluToHToZZTo2L2Q_M-250_7TeV-powheg-pythia6	156.63	1915.27
GluGluToHToZZTo2L2Q_M-275_7TeV-powheg-pythia6	134.23	2193.46
GluGluToHToZZTo2L2Q_M-300_7TeV-powheg-pythia6	117.81	2514.96
GluGluToHToZZTo2L2Q_M-325_7TeV-powheg-pythia6	108.12	2624.88
GluGluToHToZZTo2L2Q_M-350_7TeV-powheg-pythia6	108.99	2699.44
GluGluToHToZZTo2L2Q_M-375_7TeV-powheg-pythia6	102.40	2779.99
GluGluToHToZZTo2L2Q_M-400_7TeV-powheg-pythia6	83.17	3606.95
GluGluToHToZZTo2L2Q_M-425_7TeV-powheg-pythia6	70.46	4139.36
GluGluToHToZZTo2L2Q_M-450_7TeV-powheg-pythia6	49.42	5837.91
GluGluToHToZZTo2L2Q_M-475_7TeV-powheg-pythia6	41.29	7136.59
GluGluToHToZZTo2L2Q_M-500_7TeV-powheg-pythia6	34.72	8473.64
GluGluToHToZZTo2L2Q_M-525_7TeV-powheg-pythia6	29.03	9872.98
GluGluToHToZZTo2L2Q_M-550_7TeV-powheg-pythia6	24.48	11950.92
GluGluToHToZZTo2L2Q_M-575_7TeV-powheg-pythia6	17.42	17214.30
GluGluToHToZZTo2L2Q_M-600_7TeV-powheg-pythia6	14.73	19637.09

Table 3: Signal Monte Carlo samples used in the analysis. Muon, electron, and tau final states in the leptonic Z decay are considered. The total branching fraction $\mathrm{BR}_{2l2j}(\mathrm{ZZ} \to 2\ell 2\mathrm{j}) = 2 \times 0.101 \times 0.699 = 0.139$ is used. Both the gluon fusion and weak boson fusion mechanisms are considered in the cross section calculation. Higgs production cross sections and branching ratios of Higgs to ZZ are taken from the CERN yellow report [9].

2.3 Data Samples

We are using the double lepton primary datasets corresponding to 4 fb^{-1} of data collected in 2011. We also use the Muon-Electron primary dataset for the determination of the $t\bar{t}$ background from data. The data sample is a mixture of promtpt reconstruction and reprocessing passes for different periods. The data samples are listed in Table 4.

Dataset name
/DoubleMu/Run2011A-May10ReReco-v1/AOD
/DoubleMu/Run2011A-PromptReco-v4/AOD
/DoubleMu/Run2011A-05Aug2011-v1/AOD
/DoubleMu/Run2011A-PromptReco-v6/AOD
/DoubleMu/Run2011B-PromptReco-v1/AOD
/DoubleElectron/Run2011A-May10ReReco-v1/AOD
/DoubleElectron/Run2011A-PromptReco-v4/AOD
/DoubleElectron/Run2011A-05Aug2011-v1/AOD
/DoubleElectron/Run2011A-PromptReco-v6/AOD
/DoubleElectron/Run2011B-PromptReco-v1/AOD
/MuEG/Run2011A-May10ReReco-v1/AOD
/MuEG/Run2011A-PromptReco-v4/AOD
/MuEG/Run2011A-05Aug2011-v1/AOD
/MuEG/Run2011A-PromptReco-v6/AOD
/MuEG/Run2011B-PromptReco-v1/AOD

Table 4: 2011 data samples.

3 Event Selection

The main signature of $H \to ZZ \to 2\ell 2j$ is the presence of a lepton pair and a jet pair having an invariant mass around the Z mass. The width of the invariant mass is dominated by the Z intrinsic width for the di-lepton pair, and by the jet resolution for the jet pair. The Higgs boson mass can be reconstructed as the invariant mass of the four objects in the final state, $m_{\ell\ell jj}$.

The main background to this channel is the SM production of Z in association with jets. This background can be reduced requiring the identification (tagging) of the two final jets as b jets, hence restricting the Higgs decay to $H \to ZZ \to 2\ell 2b$. Production of Z boson pairs and $t\bar{t}$ also contribute to the total background. ZZ production can be reduced exploiting the significant boost of the Z bosons coming from the Higgs decay, when the Higgs mass is significantly larger than $2\,m_Z$. $t\bar{t}$ events have a significant missing transverse energy ($\not{E}_T$) due to the presence of the neutrinos in the final state that is not present in the Higgs signal.

In the following sub-sections we describe the selection of leptons and b-jets, then in a dedicated section we present the kinematic selection adopted to reduce the SM backgrounds.

3.1 Preselection

We select events with 2 leptons and 2 jets according to the lepton and jet selection described in the following Sections. We don't apply b-tagging requirements at the pre-selection stage. We also select events with only one jet for background control purposes. All events are required to have a di-lepton invariant mass $m_{\ell\ell}$ greater than 50 GeV.

Isolation is an important variable to distinguish leptons from EW processes from the ones from QCD background and b-decays. We define isolation variables for the tracker, electromagnetic and hadronic calorimeters as follows: $I_{\text{trk}} = \sum_{\text{tracks}} p_T$, $I_{\text{ECAL}} = \sum_{\text{ECAL}} E_T$, $I_{\text{HCAL}} = \sum_{\text{HCAL}} E_T$, where the sums are performed on all objects falling within a cone $\Delta R = \sqrt{\Delta\eta^2 + \Delta\phi^2} = 0.3$ around the lepton candidate momentum direction. The energy deposits and the track associated to the lepton candidate are excluded from the sums. We ensure lepton isolation applying

cuts on the relative combined isolation, defined as:

$$R = (I_{\text{ECAL}} + I_{\text{HCAL}} + I_{\text{trk}}) / p_T.$$

3.1.1 Muons

We select global muon pairs with p_T greater than 20 GeV and 40 GeV, for the lower and greater momentum lepton respectively, and $|\eta| < 2.4$. We require the following quality selection recommended in previous studies [10]:

- Normalized χ^2 of the global track < 10
- At least 10 tracker hits
- At least 1 pixel hit
- At least 1 hit in the muon subsystem
- At least 2 matched muon stations
- Transverse impact parameter with respect to the primary vertex, $d_{xy} < 0.02$ cm
- Combined relative isolation $R < 0.15$

The transverse impact parameter cut has been tightened w.r.t. Ref. [10] in order to reduce the possible background coming from muons produced in the decays of heavy flavour mesons.

3.1.2 Electrons

We select GSF electrons with p_T greater than 20 GeV and 40 GeV, for the lower and greater momentum lepton respectively, and $|\eta| < 2.5$ that fulfill the following conditions [11]:

- Electron rejection if $1.4442 < |\eta| < 1.566$ (no electrons in the EB/EE gap)
- WP95 requirements with combined isolation $R < 0.15$

WP95 is defined in Ref. [11], and refer to two sets of cuts on electron's discriminating variables and isolation variables I_{trk}/E_T, I_{ECAL}/E_T and I_{HCAL}/E_T, that have a selection efficiency of approximately 95%.

3.1.3 Jets

Particle Flow jets [12] reconstructed with the anti-k_T [13] algorithm with radius $R = 0.5$ are considered in this analysis. Selected jets must have $p_T > 30$ GeV and $|\eta| < 2.4$.

Jet energy corrections are applied at L2 and L3. Corrections at L1, taking into account pile-up effects, are also included as default in the 2011 data.

The selected jets (j) are cleaned-up vetoing the presence of selected leptons (ℓ) within a cone around the jet by applying the cut $\Delta R(\ell, \text{j}) > 0.5$.

3.2 b-tagging requirements

After the pre-selection described in Section 3.1, heavy flavor tagging requirements are applied. Since our signal has two b-jets in the final state, the double-tag selection was found to be optimal improving the signal to background ratio. Therefore, we define three exclusive regions:
a double tag region requiring at least two b-tagged jets in the event, a single tagged region requiring that one of the two jets is a b-tagged jet, and a zero tagged region containing all the remaining events.

These three regions are the baseline selection for the analysis.

The tagging algorithm used as default in the analysis is the Track Counting High Efficiency (TCHE) [14]. For the double tag region a combination of two working points is used, requiring one of the jets being tag with the medium working point (TCHEM), and the other jet with the loose working point (TCHEL). For the single tag region one of the jets is required to be TCHEL, and the other jet is required to have a b-tag discriminator value $<$ TCHEM. These working points were chosen based on the tagging studies described in Appendix A.

Other algorithms, like Simple Secondary Vertex (SSV), performance variations (High Efficiency or High Purity), and working points (Loose, Medium, and Tight) are also checked but they are not used for the baseline results.

The b-tagging efficiencies, scale factors data/Monte Carlo, and uncertainties can be found in the following references [15] [16] provided by the BTV POG. Some numbers for our default working points are summarized in table 5. Scale factors data/Monte Carlo for b-jets and light jets misidentified as b-jets are computed as a function of p_T and η of the jets and are extracted from the official DB.

Tagger	ϵ_b^{tag} PtRel	SF_b PtRel	ϵ_b^{tag} System8	SF_b System8	ϵ_b^{tag} FtCM	SF_b FtCM
TCHEL	0.76 ± 0.01	0.95 ± 0.01	0.77 ± 0.01	0.96 ± 0.02	0.76	0.94 ± 0.01
TCHEM	0.63 ± 0.01	0.93 ± 0.02	0.63 ± 0.02	0.93 ± 0.02	0.69	0.96 ± 0.01

Table 5: Measured tagging efficiencies for b jets and data/MC scale factors for the b-tagging algorithm and operating points used in the analysis. Results for the muon-jet p_T between 50 and 80 GeV are indicated for the PtRel, System8, and FtMC methods. Information extracted from [15] and [16]

3.3 Missing Transverse Energy

At the first stage of the analysis, requiring 2 b-tagged jets and no further selection, one of the main sources of background is the $t\bar{t}$ production. These $t\bar{t}$ events contain two real b-jets and a significant amount of $\not{E}_T$ originated from neutrinos.

We reduce substantially the presence of $t\bar{t}$, while keeping the signal, requiring particle flow MET-Significance < 10. The MET-Significance distribution after double b-tagging requirements is shown in Figure 1.

3.4 Angular Information

Since the Higgs boson carries no spin, the angular distribution of its decay products is independent of the production mechanism. The five angles that fully describe the kinematics of the $gg \to H \to ZZ \to \ell^-\ell^+q\bar{q}$ process are shown in Fig. 2.

Taking advantage of this angular information a couple of methods, based on an helicity Likelihood Discriminant (LD) and on Neural Network, were explored to separate signal and background. The method and its validation are described in Section 7 and Reference [17].

4 Data-MC Comparison

Every time new data is available we check if the CMS simulation reproduce it in the preselection region described in Section 3.1.

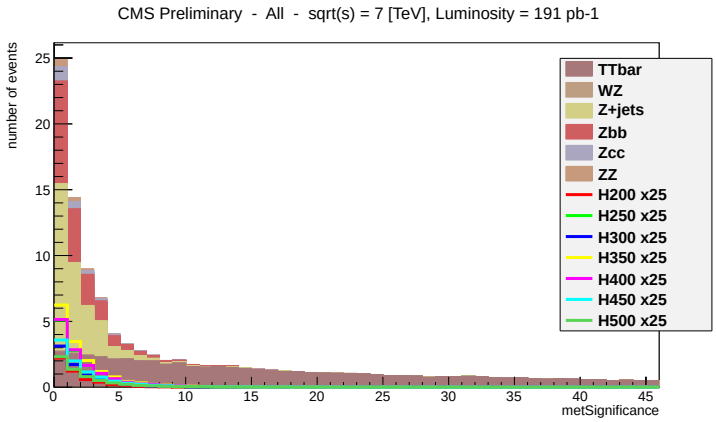

Figure 1: MET-Significance distribution for several Higgs masses (lines) and backgrounds (stacked histograms).

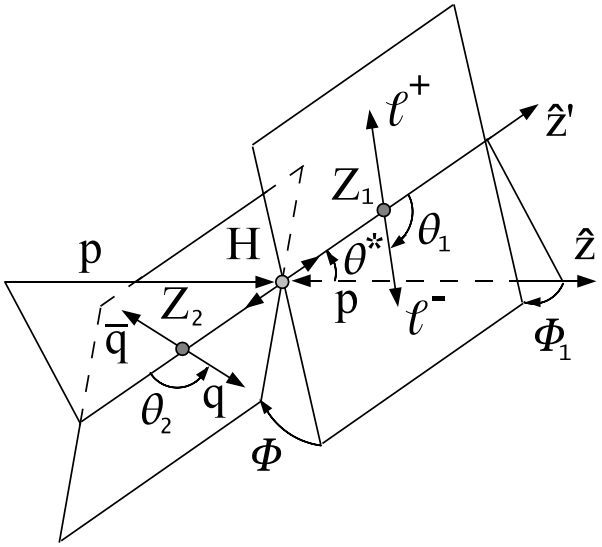

Figure 2: Diagram describing the production and decay angles in the process $gg \to H \to ZZ \to \ell^-\ell^+q\bar{q}$. These angles are defined in the parent particle rest frames (H or Z).

4.1 2011A Data

The m_{jj}, m_{ll}, and MET-Significance distributions are shown in Figures 10 to 12 for a 2.1 fb^{-1} of data from the 2011A period.

Also distributions of the TCHE discriminator are shown in Figures 6.

Distributions of the angular variables used in the helicity LD, and the helicity LD itself, are also checked as shown in Figures 13 to 15. These distributions are checked after preselection and tagging requirements.

4.2 2011B Data

The m_{jj}, m_{ll}, MET-Significance, and TCHE distributions are shown in Figures 10 to 12 for a 1.8 fb^{-1} of data from the 2011B period.

Distributions of the angular variables used in the helicity LD, and the helicity LD itself, are also

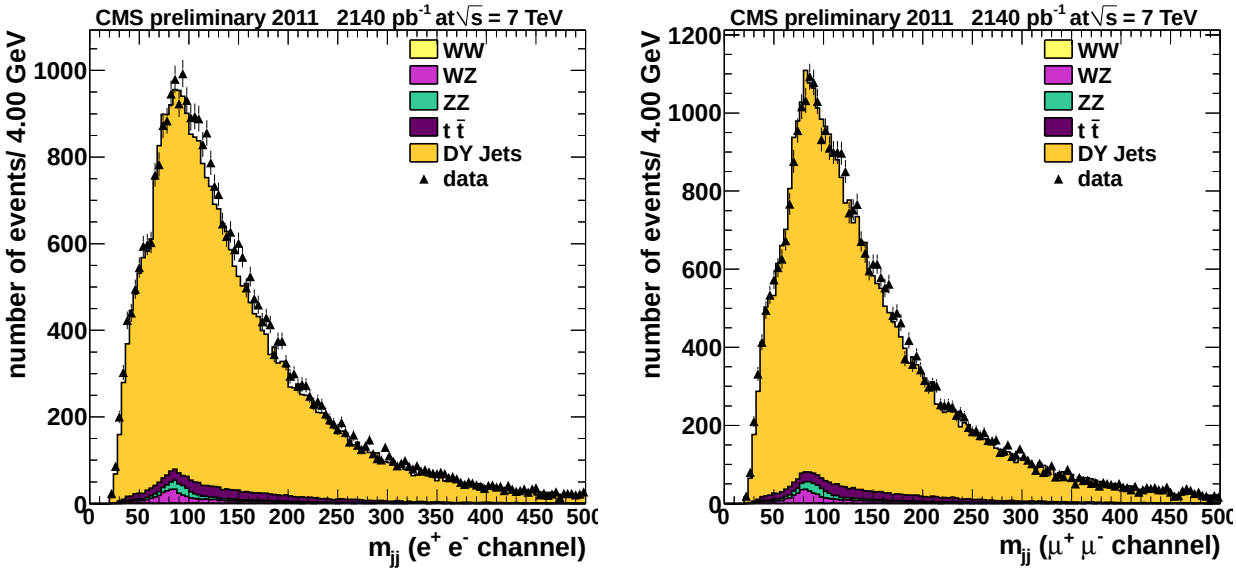

Figure 3: Distribution of the m_{jj} for electron (left) and muon (right) events in 2.1 fb^{-1}, 2011A.

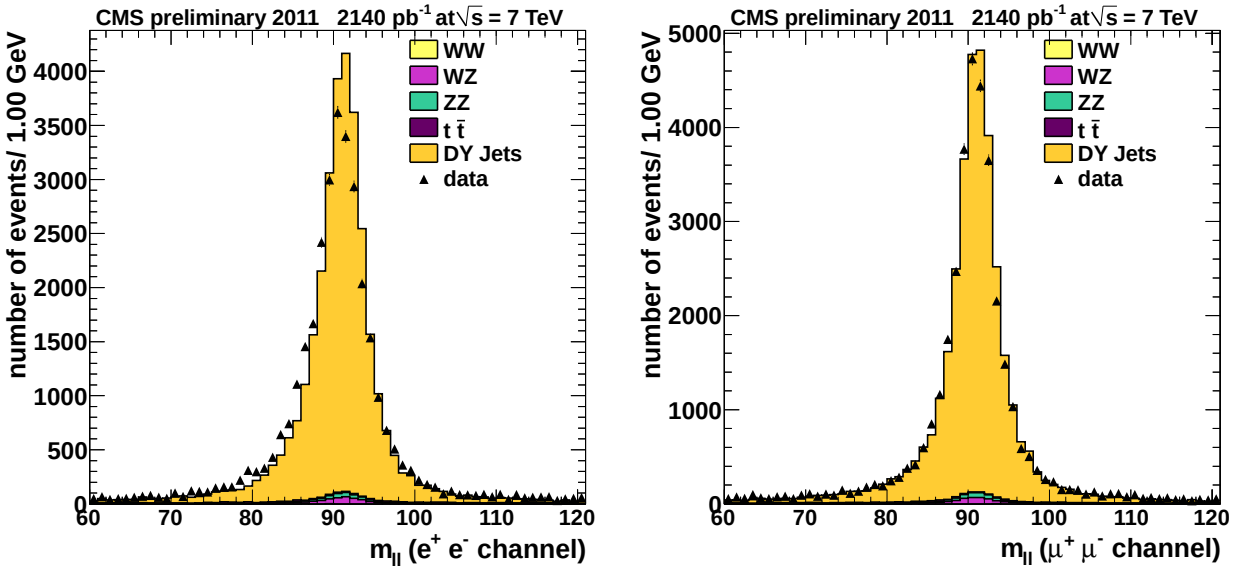

Figure 4: Distribution of the m_{ll} for electron (left) and muon (right) events in 2.1 fb^{-1}, 2011A.

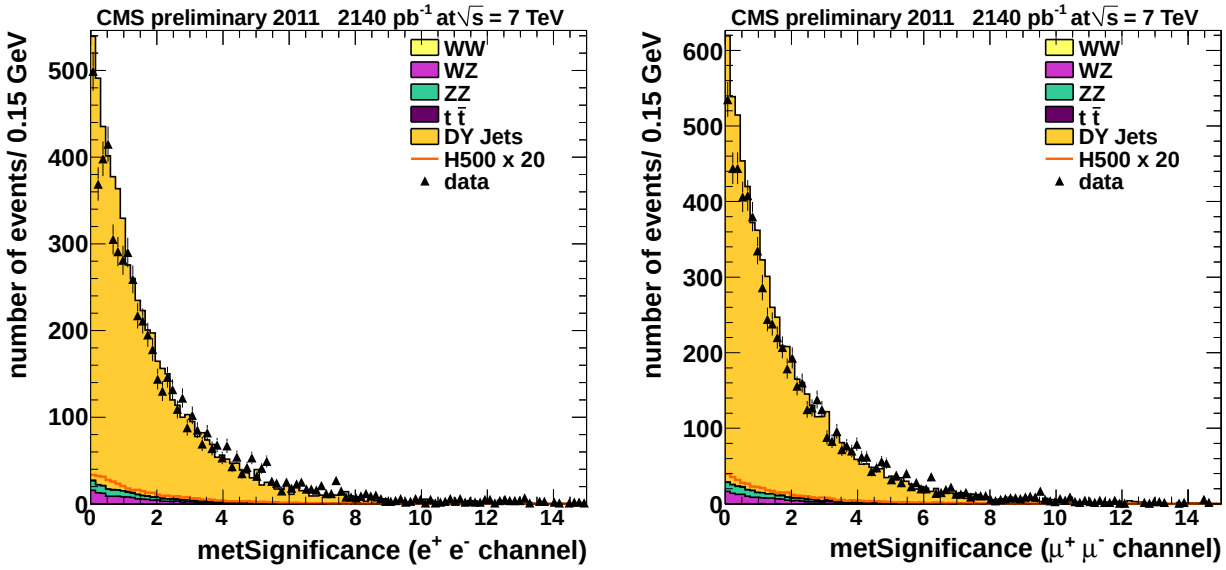

Figure 5: Distribution of the MET-Significance for electron (left) and muon (right) events in 2.1 fb^{-1}, 2011A.

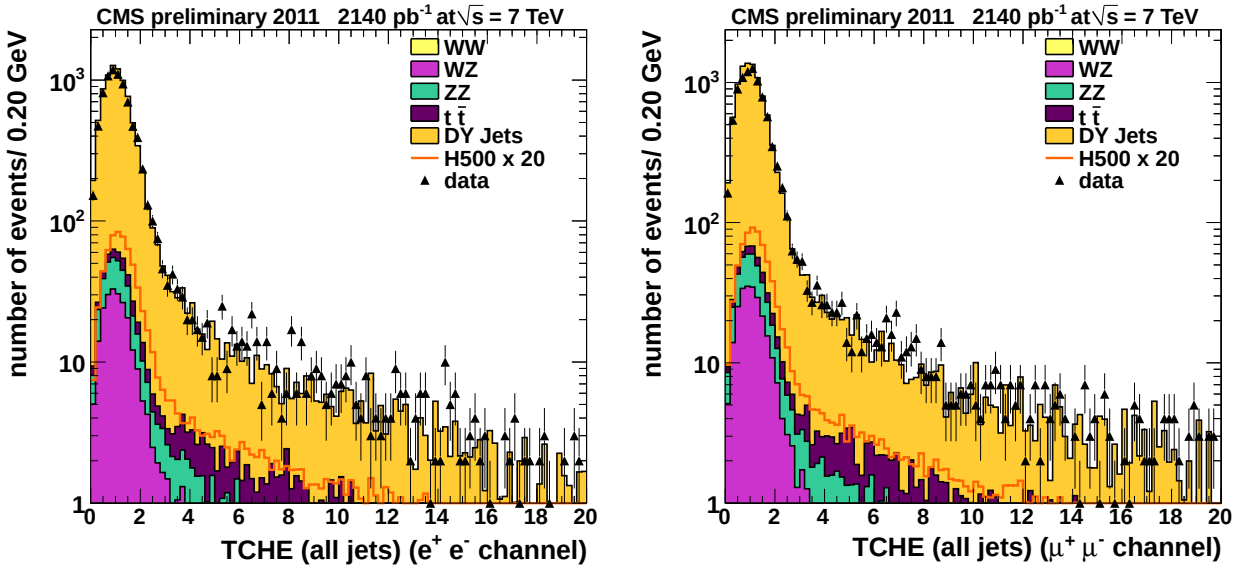

Figure 6: Distribution of the TCHE discriminator for electron (left) and muon (right) events in 2.1 fb^{-1}, 2011A.

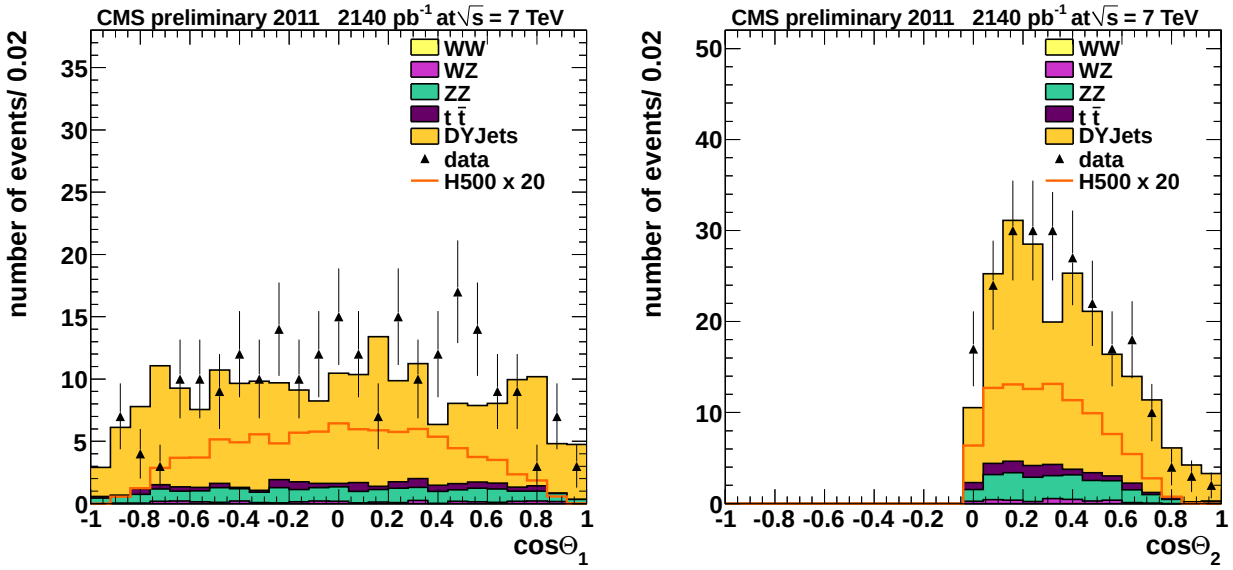

Figure 7: Distribution of the $cos\theta_1$ (left) and $cos\theta_2$ (right) events in 2.1 fb^{-1}, 2011A.

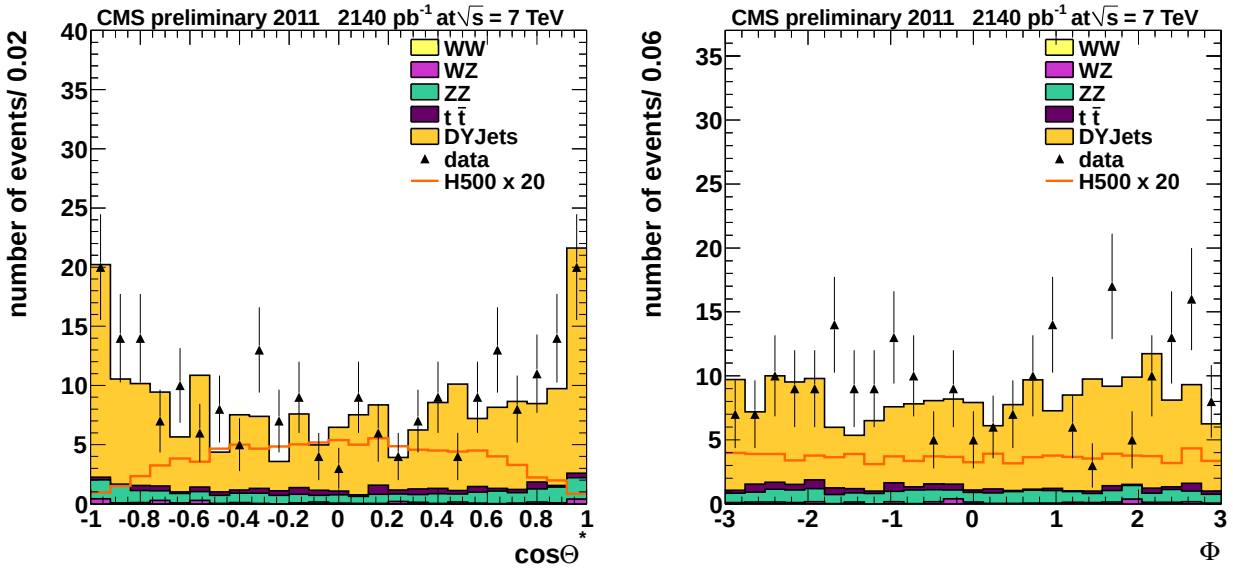

Figure 8: Distribution of the $cos\theta^*$ (left) and ϕ (right) events in 2.1 fb^{-1}, 2011A.

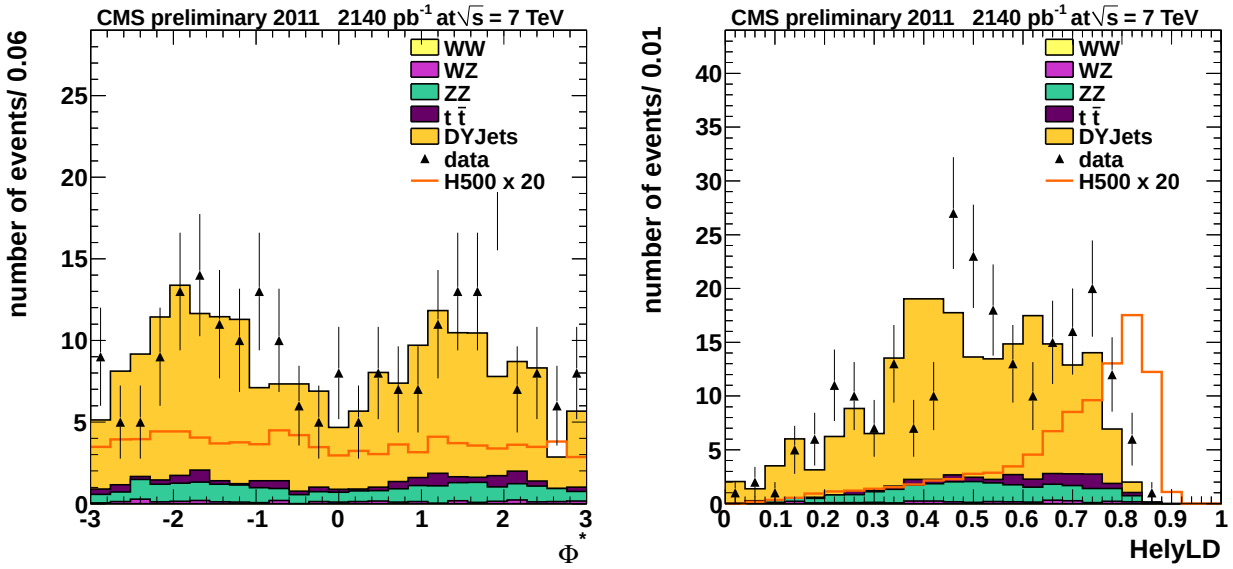

Figure 9: Distribution of the ϕ^* (left) and helicity LD (right) events in 2.1 fb^{-1}, 2011A.

checked as shown in Figures 13 to 15. These distributions are checked after preselection and tagging requirements.

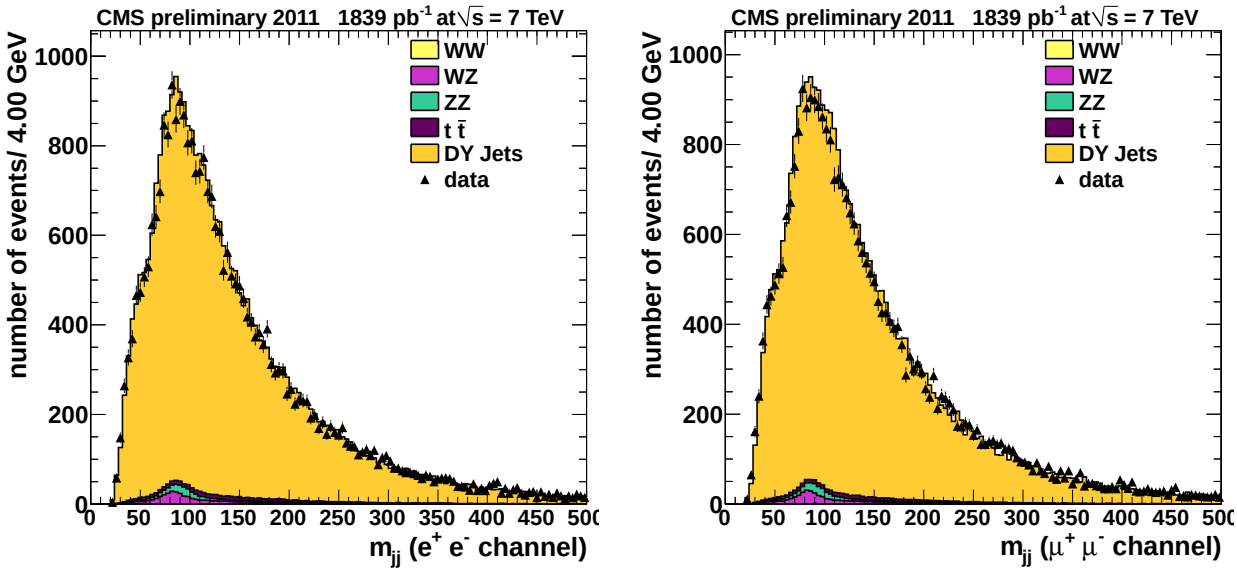

Figure 10: Distribution of the m_{jj} for electron (left) and muon (right) events in 1.8 fb^{-1}, 2011B.

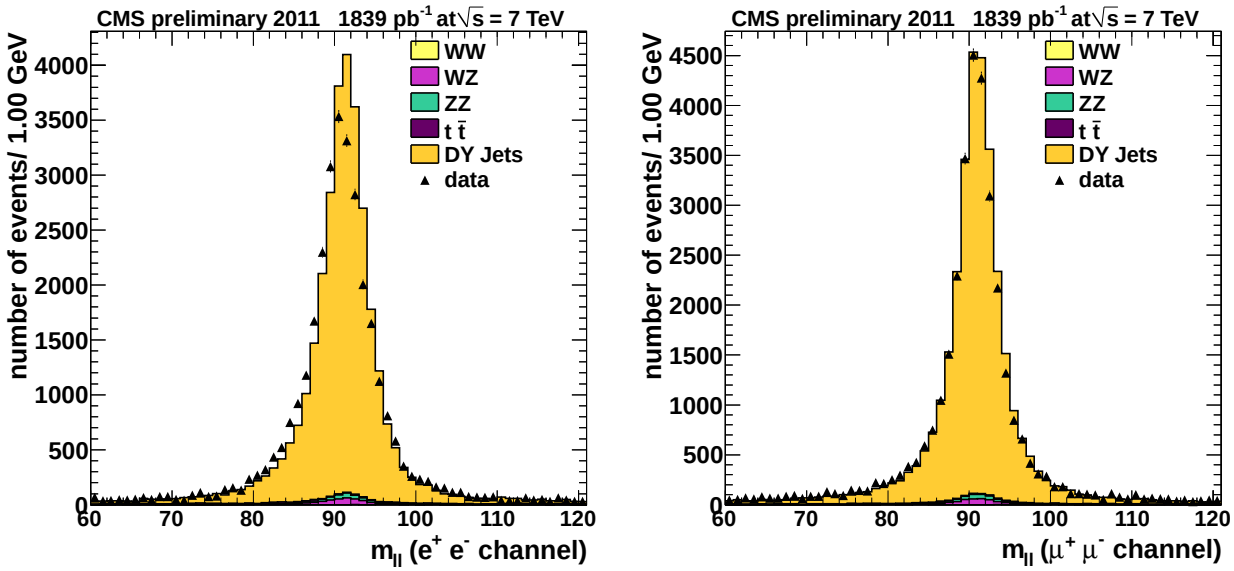

Figure 11: Distribution of the m_{ll} for electron (left) and muon (right) events in 1.8 fb^{-1}, 2011B.

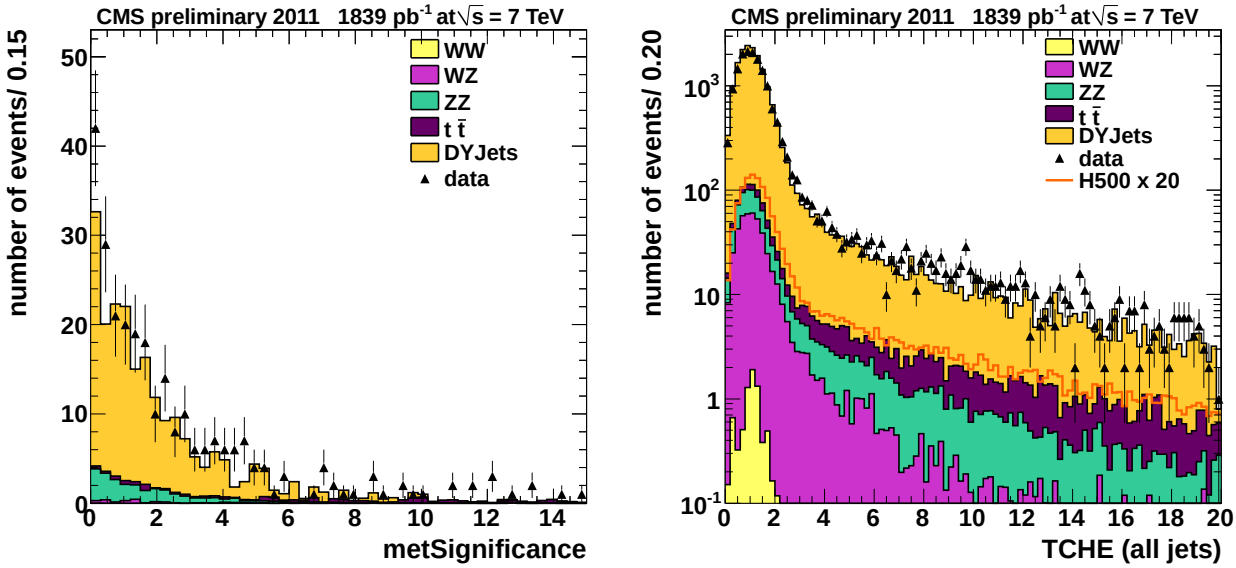

Figure 12: Distribution of the MET-Significance (left) and TCHE discriminator (right) in 1.8 fb^{-1}, 2011B.

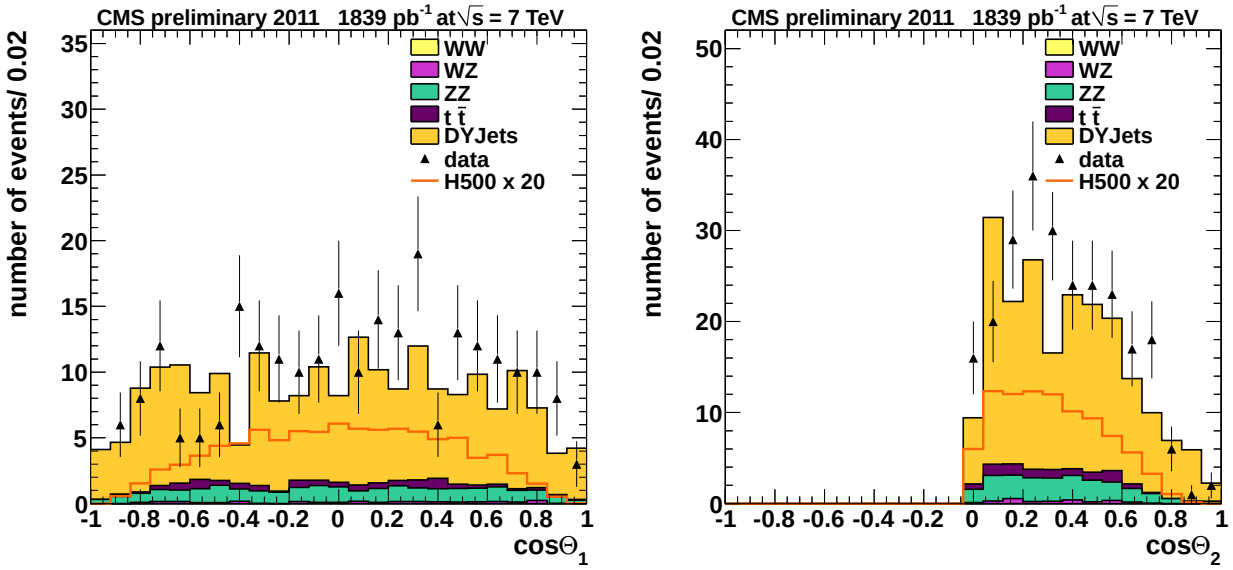

Figure 13: Distribution of the $cos\theta_1$ (left) and $cos\theta_2$ (right) events in 1.8 fb^{-1}, 2011B.

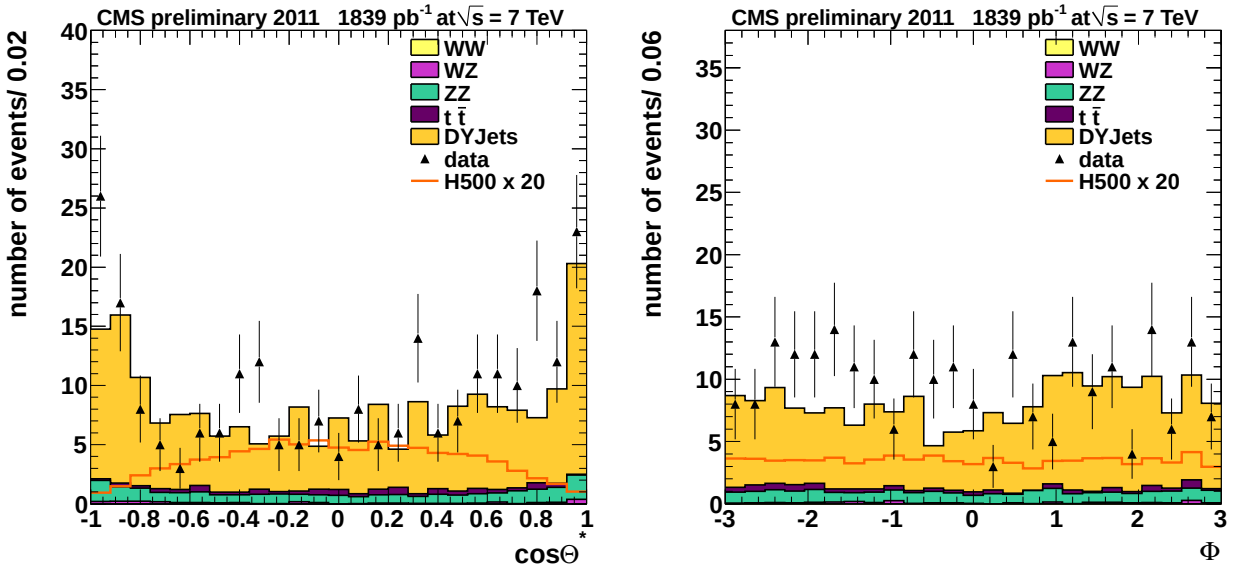

Figure 14: Distribution of the $cos\theta^*$ (left) and ϕ (right) events in 1.8 fb^{-1}, 2011B.

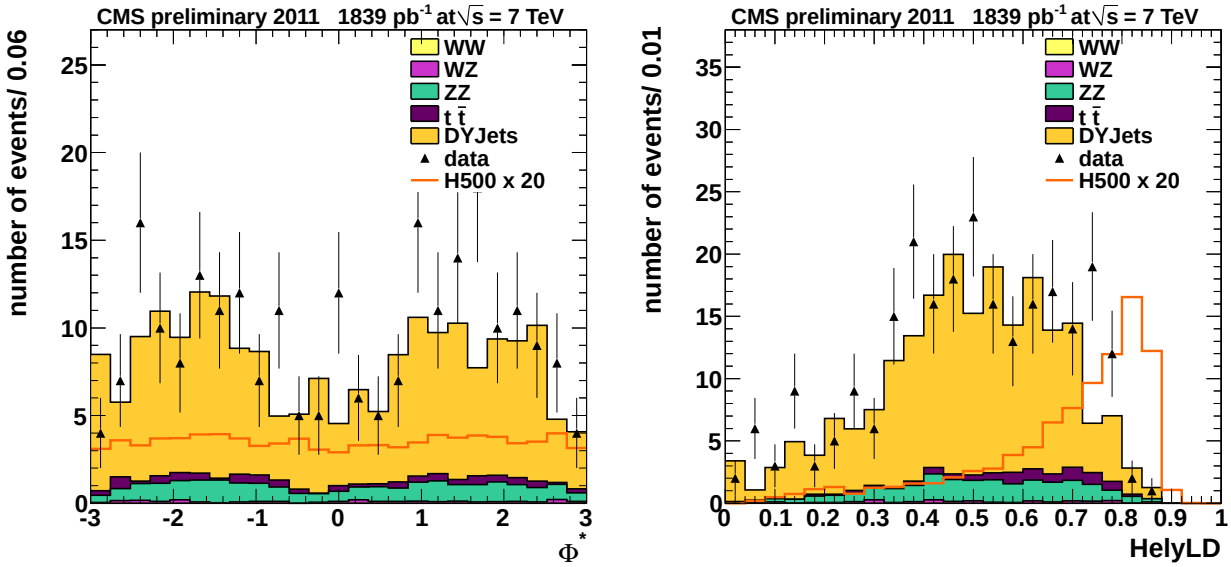

Figure 15: Distribution of the ϕ^* (left) and helicity LD (right) events in 1.8 fb^{-1}, 2011B.

5 Background Control and Cross Checks

The main procedure for background estimation from side-band data is extensively described in the complementary Analysis Note [17]. In the applied side-band method, the only place where the MC prediction plays a role is in the ratio variable between side-band and signal region. Since the main contribution is the $Z + jets$ production is a key issue in this analysis the cross check of this background using different Monte Carlo generators. A comparison using Sherpa and Madgraph is describes in this section.

The MC prediction of yields and shapes of the various relevant backgrounds are affected by theoretical uncertainties. We define, in this section of the note, a data-driven method to determine the $t\bar{t}$ background from background-enriched regions obtained by inverting some of the selection criteria.

5.1 Validation of Z+Jets sample with SHERPA Monte Carlo

Sherpa is a Monte Carlo event generator for the Simulation of High-Energy Reactions of PArticles [18] that is supposed to well reproduce the data collected in the LHC.

The validation of this Monte Carlo is important because, even though the number of expected events of background in the signal region is taken from data in the sideband region, the ratio between the expected number of events in signal and sideband region is calculated from simulation. Having different event generators allow us to estimate the systematic uncertainty in this ratio due to the simulation.

In addition, SHERPA is supposed to be richer in high flavour jet events, so the validation of this generator is very interesting for studies involving heavy flavour quarks, as it may be used it in further analysis.

In this section we have focused only in the study of important variables for this analysis. We demand the same preselection requirements plus the two leptons to be in the Z mass region, each one with $p_T > 20GeV$. The Z+Jets distribution has been normalized to data before the final selection so the total number of expected events matches the observed ones at this stage. In Figure 16 it is shown the distribution of number of jets. Madgraph reproduces better the data, as SHERPA shows a deficit of events when the number of jets is below 6.

Figure 17 shows the m_{jj} before the final selection, with good agreement between data and simulation.

The final selection includes the helicity Likelihood Discriminant and b-tagging requirements, as well as the dijet invariant mass to be in the Z mass window, and met significance < 10 in the case of the 2 b-tagged jets. Leading lepton is asked to have $p_T > 40GeV$. Q-G discriminant was not applied to the 0 b-tag category.

In Figure 18 it is shown the m_{lljj} invariant mass, both for muons (left) and electrons (right), before the final selection. The same plots are shown in Figure 19 for different b-tag categories.

Finally, in Figures 21 and 21 we compare the shape of MADGRAPH and SHERPA m_{lljj} distribution, with areas normalized to unity.

The number of expected and observed events, both for muons and electrons, are shown in tables 6 and 7, respectively.

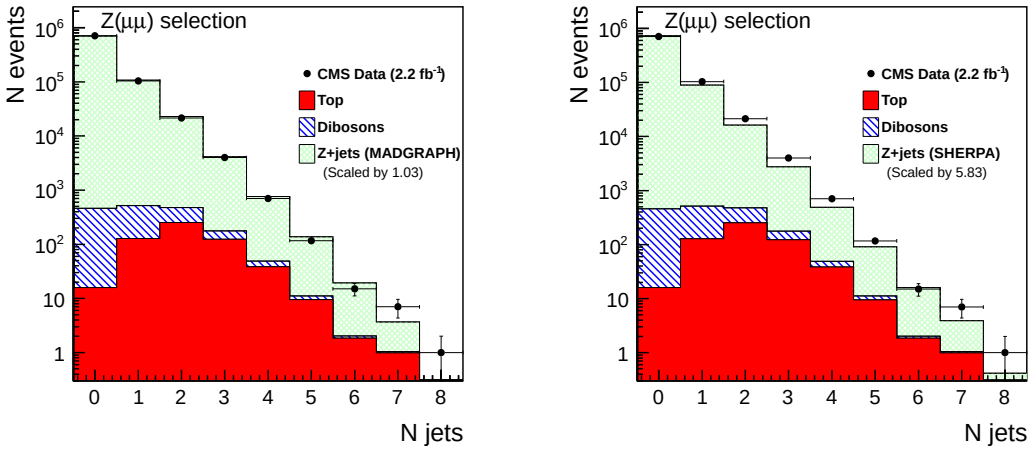

Figure 16: Distribution of the number of jets in a Z(mumu)+jets selection. Left: Madgraph Z+Jets sample Right: SHERPA Z+Jets sample

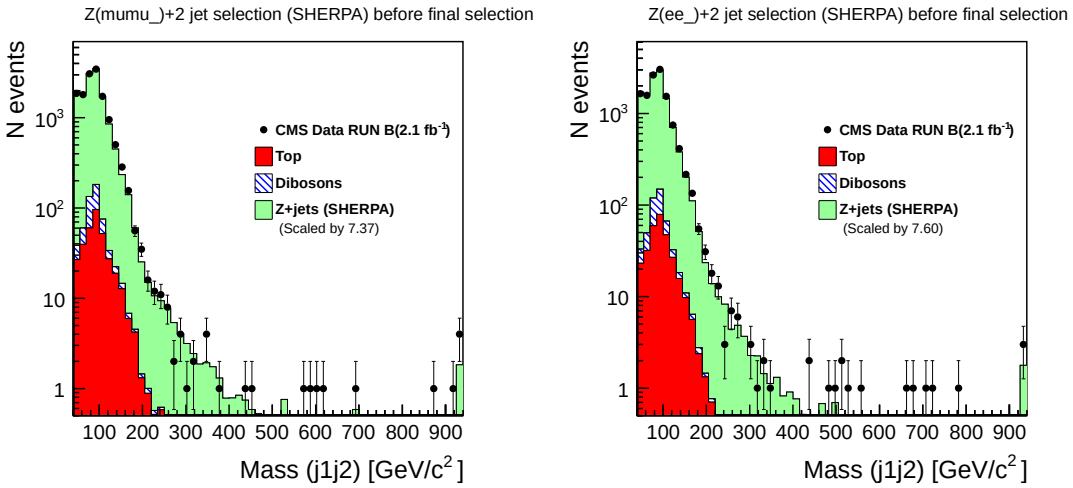

Figure 17: The m_{jj} invariant mass before the final selection for muon (left) and electron (right) events with SHERPA Z+jets generator

	Top	Diboson	Total background (Madgraph) Norm. Factor =0.93	Total background (Sherpa) Norm. Factor =7.3	Data $\int$Ldt= 2.1 fb^{-1}
Z(mumu)+2jets	348.9	229.5	14006.9	14007	14007
0 btag	8.4	24.5	901.3	789.25	855
1 btag	68.6	21.7	754.3	731.0	738
2 btag	7.5	3.7	44.8	54.7	51

Table 6: Number of expected and observed $\mu\mu$ events with diferent event selections for a luminosity of 2.1 fb^{-1}

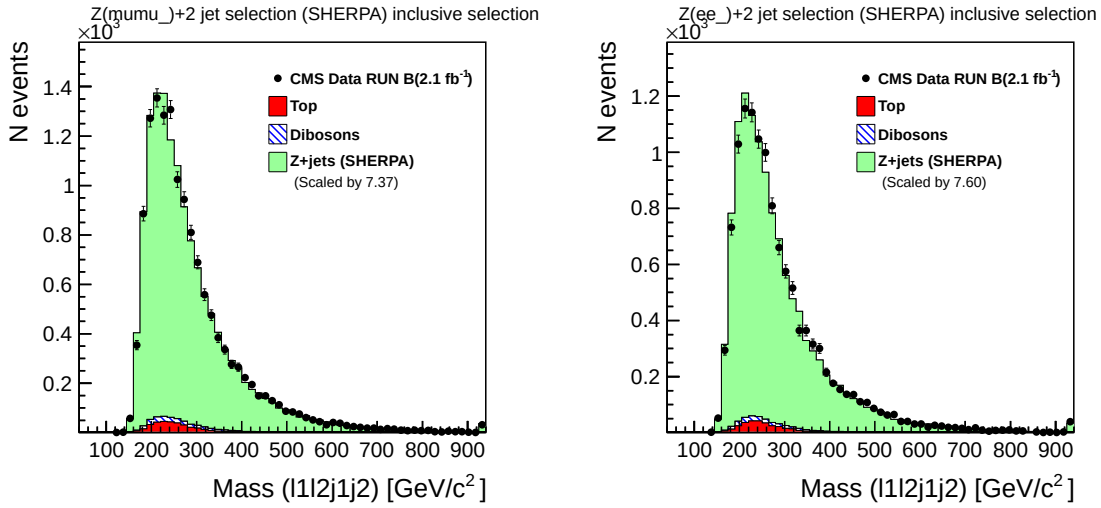

Figure 18: Expected and observed m_{lljj} distribution using SHERPA for muons (left) and electrons (right) in the preselection region.

	Top	Diboson	Total background (Madgraph) Norm. Factor =0.97	Total background (Sherpa) Norm. Factor =7.6	Data $\int$Ldt=2.1 fb^{-1}
Z(ee)+2jets	305.7	189.2	12074.9	12073.7	12075
0 btag	9.6	21.6	775.0	700.9	779
1 btag	64.9	17.5	666.6	632.6	663
2 btag	6.26	2.8	45.5	46.4	53

Table 7: Number of expected and observed *ee* events with different event selections for a luminosity of 2.1 fb^{-1}

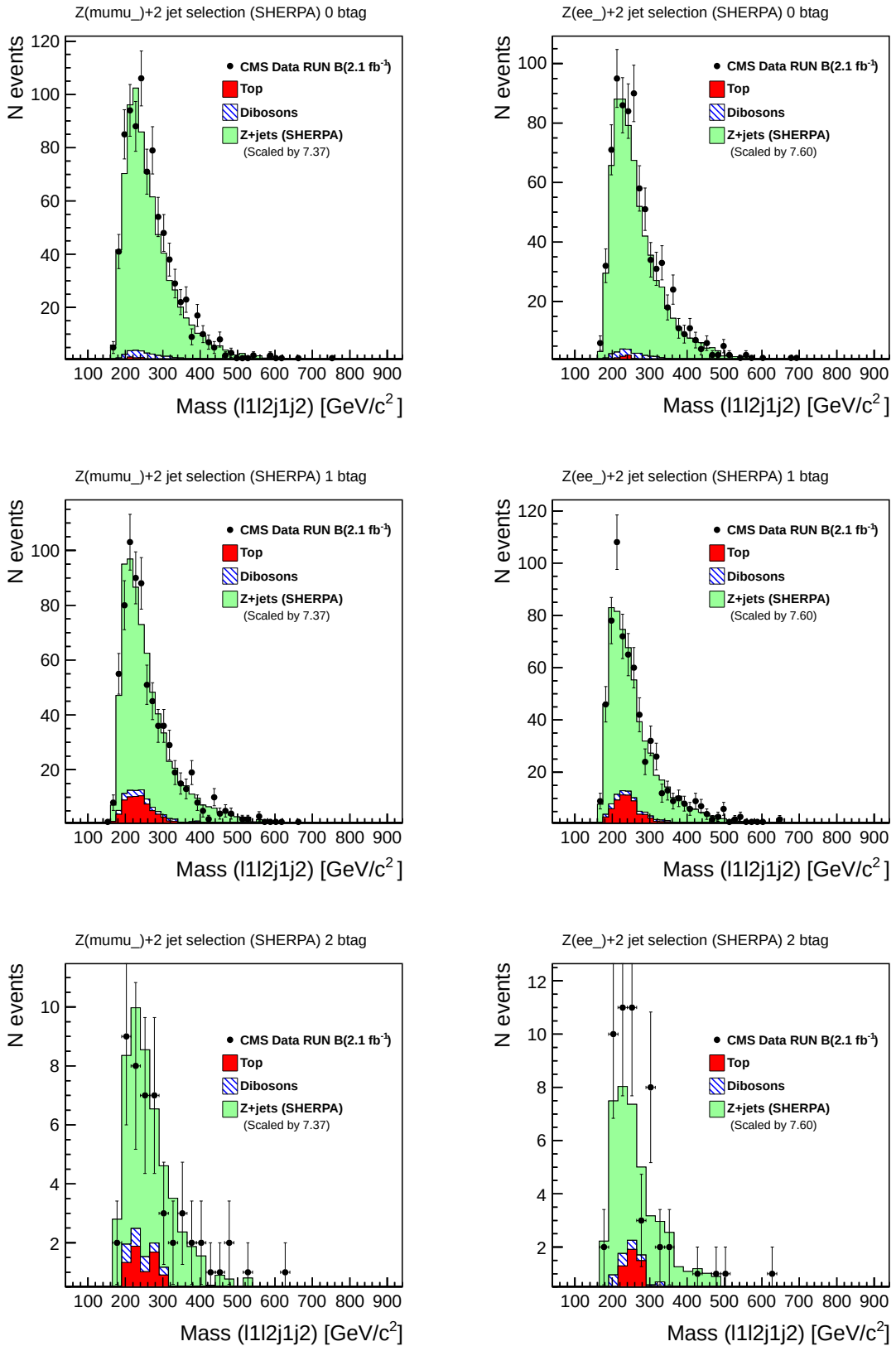

Figure 19: Expected and observed m_{lljj} distribution using SHERPA for muons (left) and electrons (right) for different final selections

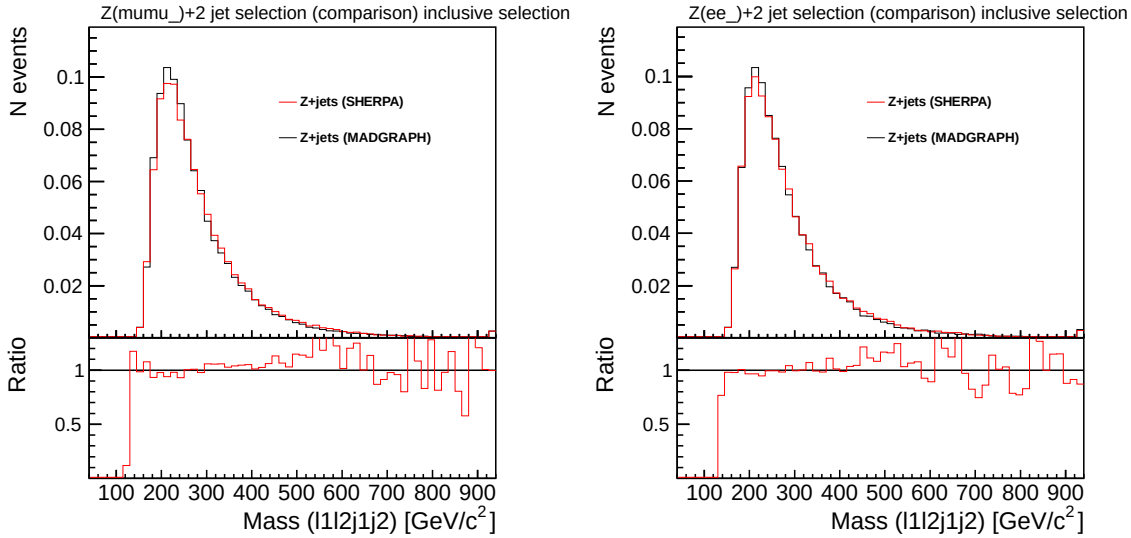

Figure 20: Comparison of m_{lljj} events distributions obtained with MADGRAPH (black) and SHERPA (red) for muons(left) and electrons (right) with 2.1 fb-1 in the preselection region.

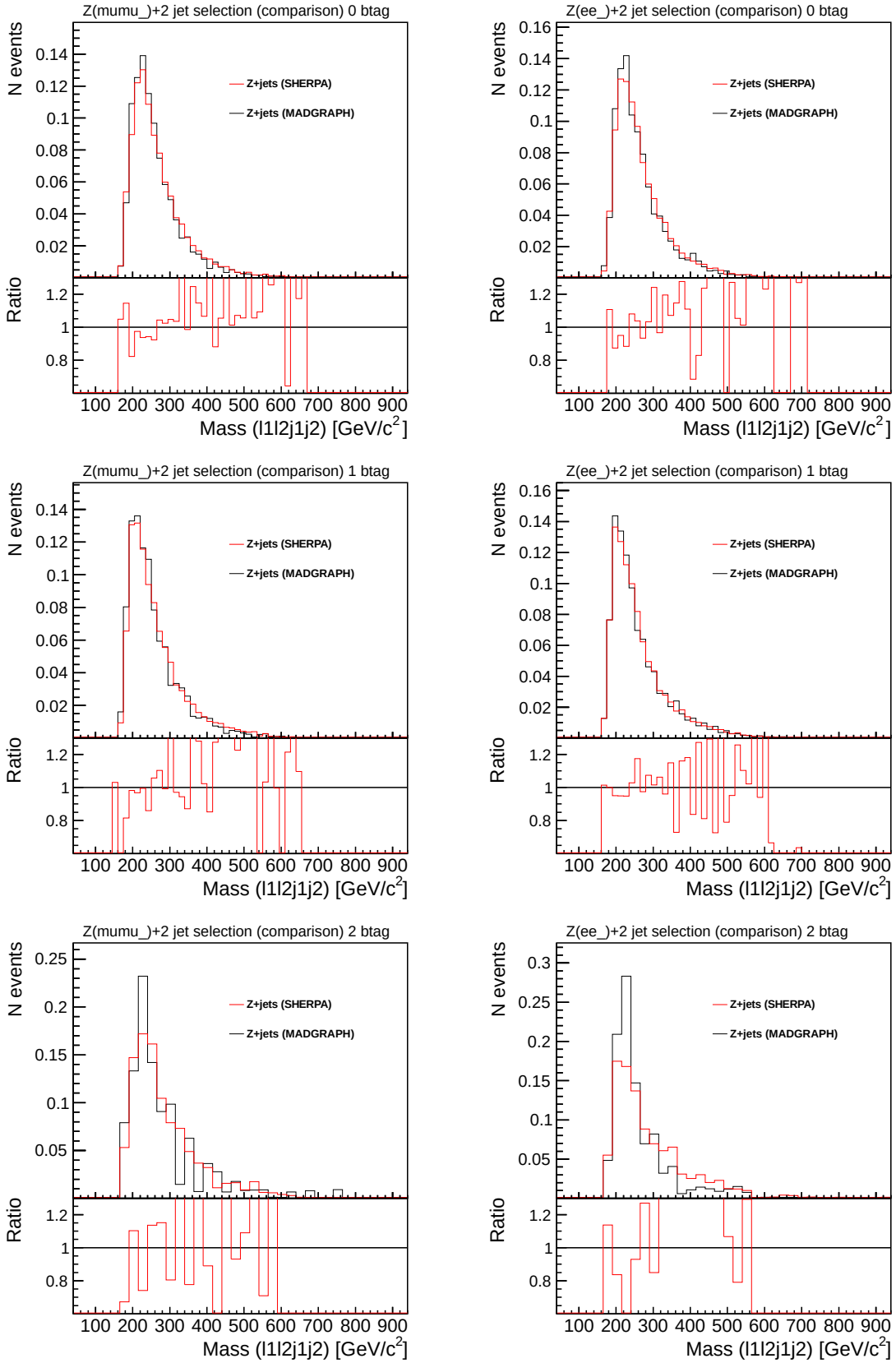

Figure 21: Comparison of m_{lljj} events distributions obtained with MADGRAPH (black) and SHERPA (red) for muons(left) and electrons (right) with 2.1 fb-1 in different tagging regions.

5.2 $t\bar{t}$ Background Determination from Data

The $t\bar{t}$ background is estimated from the data using $e\mu$ events passing the same cuts as the signal. This method accounts for other small backgrounds (as WW + jets, $Z \to \tau\tau$ + jets, single top, fakes) where the lepton flavour symmetry can be invoked as well.

In this study we used three different Monte Carlo samples: Madgraph $t\bar{t}$ inclusive sample; Powheg + Herwig $t\bar{t} \to 2l2\nu$; Powheg + Pythia $t\bar{t} \to 2l2\nu$ sample populated with one order of magnitude more events with respect to the others.

Top-pair Monte Carlo studies show that the $e\mu$ vs. $ee + \mu\mu$ symmetry works very well at the level of the shapes of the distributions of all considered variables. Also, the relative event normalization is consistent with one, within the MC finite statistical errors. For instance, in the case of Powheg + Pythia top MC, the $e\mu/(ee + \mu\mu)$ relative event normalizations are 0.999 ± 0.002 after selection and kinematical cuts, and 1.006 ± 0.009 after b-tagging.

Figure 22 shows a comparison of the $ee + \mu\mu$ and $e\mu$ top MC distributions of several relevant variables, for events with at least two leptons and two jets passing selection cuts. Only the hardest-$\sum P_T$ dilepton combination, and the dijet combination with largest TCHE discriminator values are considered. The selection step is specified in each plot. The category "$\geq$ 1 b-tag" includes events with at least one jet tagged using TCHEL prescription. The category "2 b-tag" includes events with one jet tagged using TCHEM prescription and one jet tagged using TCHEL. The normalization is arbitrary.

Cuts	Top MC	Total MC	$e\mu$ data
$M_{ll} > 50$ GeV/c^2	4873.1	5635.1	5856
70 GeV/$c^2 < M_{ll} < 110$ GeV/c^2	1713.4	2029.3	2095
70 GeV/$c^2 < M_{jj} < 110$ GeV/c^2	384.0	471.5	489
≥ 1 TCHEL b-tagged jet	353.3	398.9	425
≥ 1 TCHEM b-tagged jet	320.8	349.5	368
≥ 1 TCHEL & ≥ 1 TCHEM	195.1	201.8	211
MET Significance < 10	54.9	58.0	62
Angular LD > 0.5	39.7	41.0	39

Table 8: Comparison of 2011 $e\mu$ data to Powheg + Herwig top MC event yields, corresponding to an integrated luminosity of 4.6 fb^{-1}. "Total MC" contains the top, WW, $Z \to \tau\tau$, single top, and fakes contributions. Every cut in a line assumes all cuts in lines above.

The 2011 $e\mu$ data yield is compared to the sum of top MC prediction and other small backgrounds in Tables 8-10 while distributions of relevant variables are superimposed in Figures 23-26. Events selected contain at least two leptons and two jets passing selection cuts. Only the hardest-$\sum P_T$ dilepton combination and the dijet combination with largest TCHE discriminator values are considered. Pile-up corrections have been applied. Other extra cuts are detailed where appropriate.

The tables and figures above include an estimation of WW, $Z \to \tau\tau$, and single top contributions from Monte Carlo. The fake component is estimated from $e\mu$ data; the yield of events with one or two non-isolated leptons (in the combined relative isolation region 0.25 - 1.), is extrapolated into the isolated lepton region assuming a flat distribution in the combined relative isolation variable. This hypothesis is supported by the data. The $e - \mu$ symmetry holds in good approximation for the non-isolated lepton data.

Differences between different top MC predictions are important in term of normalization, as

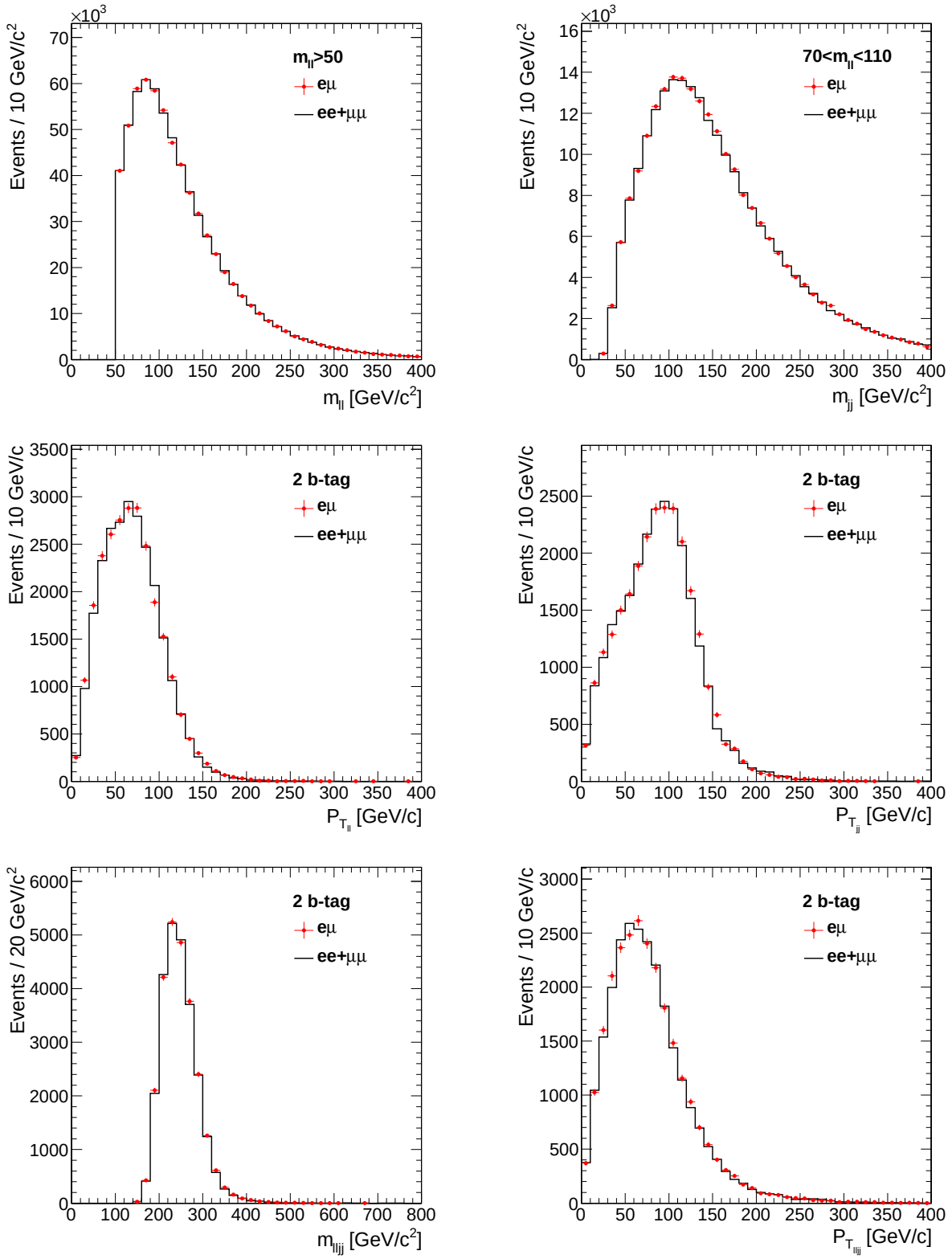

Figure 22: Powheg + Pythia top MC $e\mu$ to $(ee + \mu\mu)$ comparison for several variables after different step of the selection, as specified in the legends. Top: di-lepton invariant mass (Left) and di-jet invariant mass. Center: di-lepton (left) and dijet transverse momentum (right). Bottom: di-lepton + di-jet "Higgs" invariant mass (left) and transverse momentum (right).

Cuts	Top MC	Total MC	$e\mu$ data
$M_{ll} > 50\ \mathrm{GeV}/c^2$	5180.1	5942.2	5856
$70\ \mathrm{GeV}/c^2 < M_{ll} < 110\ \mathrm{GeV}/c^2$	1857.2	2173.1	2095
$70\ \mathrm{GeV}/c^2 < M_{jj} < 110\ \mathrm{GeV}/c^2$	398.1	485.5	489
≥ 1 TCHEL b-tagged jet	365.5	411.1	425
≥ 1 TCHEM b-tagged jet	324.8	353.5	368
≥ 1 TCHEL & ≥ 1 TCHEM	195.1	201.7	211
MET Significance $< 10.$	59.2	62.3	62
Angular LD > 0.5	40.2	41.5	39

Table 9: Comparison of 2011 $e\mu$ data to Madgraph top MC event yields, corresponding to an integrated luminosity of 4.6 fb^{-1}. "Total MC" contains the top, WW, $Z \to \tau\tau$, single top, and fakes contributions. Every cut in a line assumes all cuts in lines above.

Cuts	Top MC	Total MC	$e\mu$ data
$M_{ll} > 50\ \mathrm{GeV}/c^2$	4554.9	5316.9	5856
$70\ \mathrm{GeV}/c^2 < M_{ll} < 110\ \mathrm{GeV}/c^2$	1603.4	1919.3	2095
$70\ \mathrm{GeV}/c^2 < M_{jj} < 110\ \mathrm{GeV}/c^2$	344.5	431.9	489
≥ 1 TCHEL b-tagged jet	318.6	364.3	425
≥ 1 TCHEM b-tagged jet	283.1	311.8	368
≥ 1 TCHEL & ≥ 1 TCHEM	175.2	181.9	211
MET Significance $< 10.$	55.9	59.0	62
Angular LD > 0.5	40.1	41.3	39

Table 10: Comparison of 2011 $e\mu$ data to Powheg + Pythia top MC event yields, corresponding to an integrated luminosity of 4.6 fb^{-1}. "Total MC" contains the top, WW, $Z \to \tau\tau$, single top, and fakes contributions. Every cut in a line assumes all cuts in lines above.

can be seen in the tables. Anyway, after rescaling the several Monte Carlo using an appropriate factor, the distributions agree in shape, as illustrated in Figure 27. The rescaling factor is calculated from data before applying cuts and used in the data comparison plots. The agreement in shape is preserved even after applying more severe cuts up to the b-tag requests.

In conclusion, Powheg + Herwig and Madgraph provide a good description in terms of normalization and shape of the 2011 $e\mu$ data. Powheg + Pythia MC shows a consistent deficit in the predicted number of events but after appropriate rescaling, still agrees for what is shapes variables concerned.

Therefore, after applying the appropriate scale factor, all the Monte Carlo are equivalent. In particular, being the most populated sample, Powheg + Pythia, can be preferred to the others.

Better than using any MC would be to use the $e\mu$ sample that incorporates automatically features of the data not well simulated in the MC (the fake component, the missing transverse energy significance and angular LD distributions, efficiencies after cuts, etc).

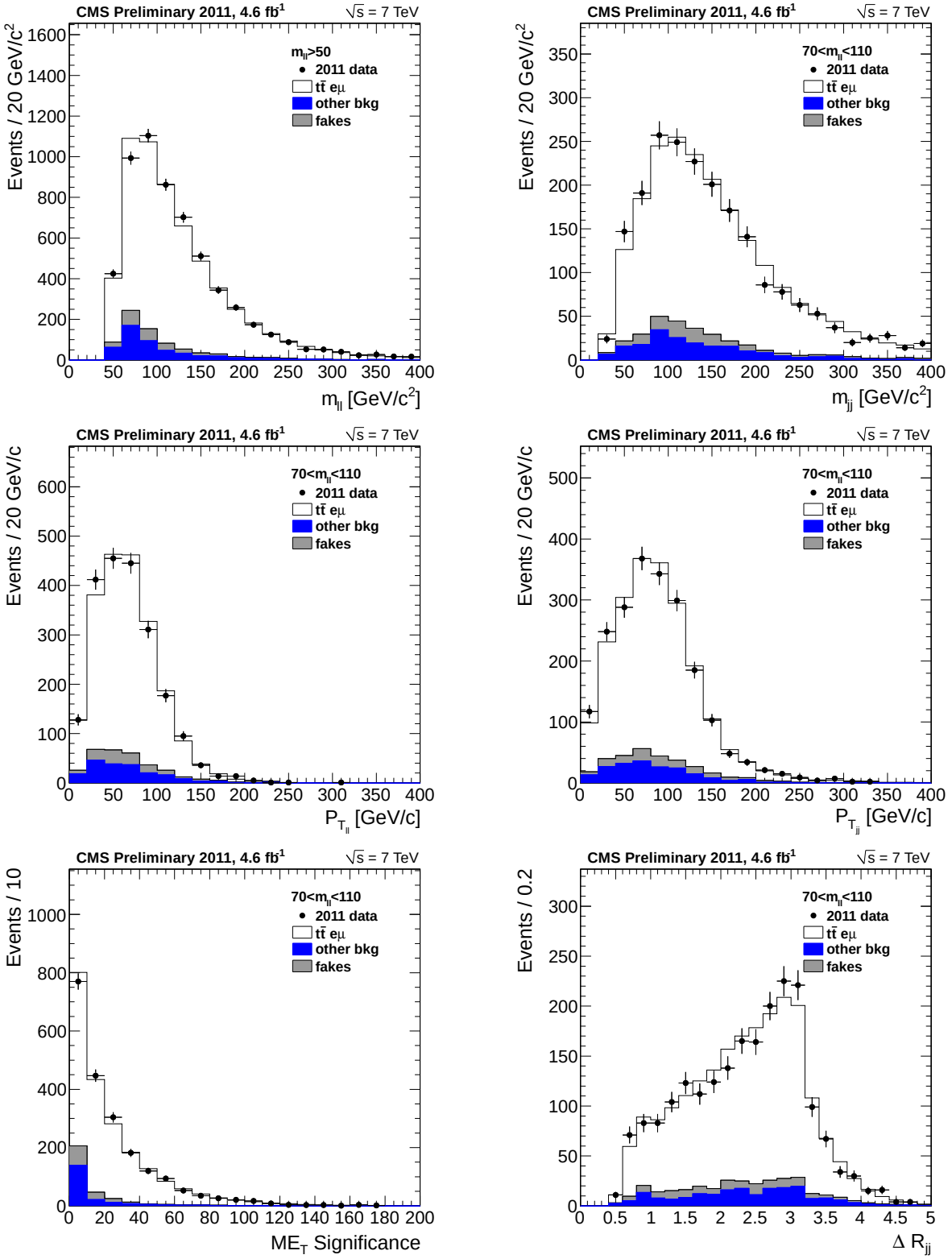

Figure 23: Comparison of 2011 $e\mu$ data to Powheg + Pythia top MC, corresponding to an integrated luminosity of 4.6 fb^{-1}. Top: dilepton invariant mass (left) and dijet invariant mass (right). Center: dilepton transverse momentum (left) and dijet transverse momentum (right). Bottom: missing transverse energy significance (left) and dijet ΔR_{jj} separation (right). Cuts described in the legends.

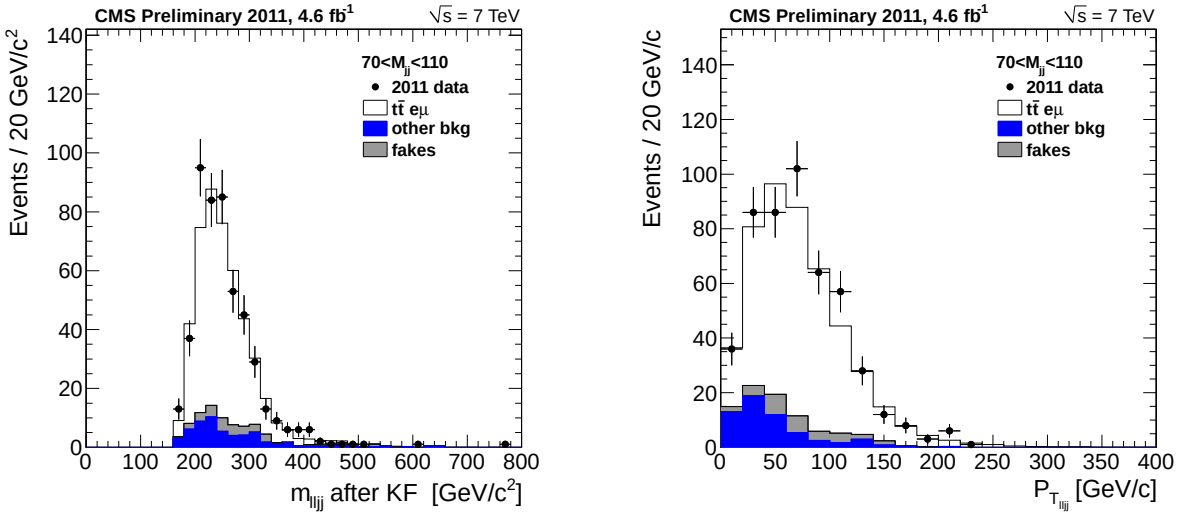

Figure 24: Comparison of 2011 $e\mu$ data to Powheg + Pythia top MC corresponding to an integrated luminosity of 4.6 fb^{-1}. Dilepton + dijet "Higgs" invariant mass (left) and transverse momentum (right) for events satisfying 70 GeV/c^2 $< M_{ll} <$ 110 GeV/c^2 and 70 GeV/c^2 $< M_{jj} <$ 110 GeV/c^2.

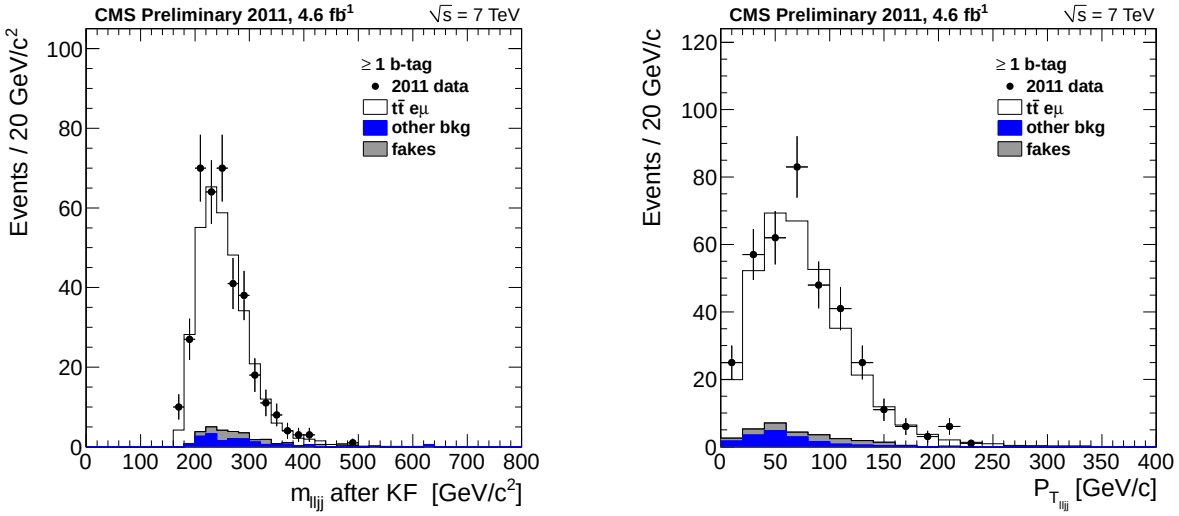

Figure 25: Comparison of 2011 $e\mu$ data to Powheg + Pythia top MC after one b-tag request, corresponding to an integrated luminosity of 4.6 fb^{-1}. Dilepton+ dijet "Higgs" invariant mass (left) and transverse momentum (right) for events satisfying 70 GeV/c^2 $< M_{ll} <$ 110 GeV/c^2 and 70 GeV/c^2 $< M_{jj} <$ 110 GeV/c^2. At lest one of the jets has been b-tagged using the TCHEM prescription.

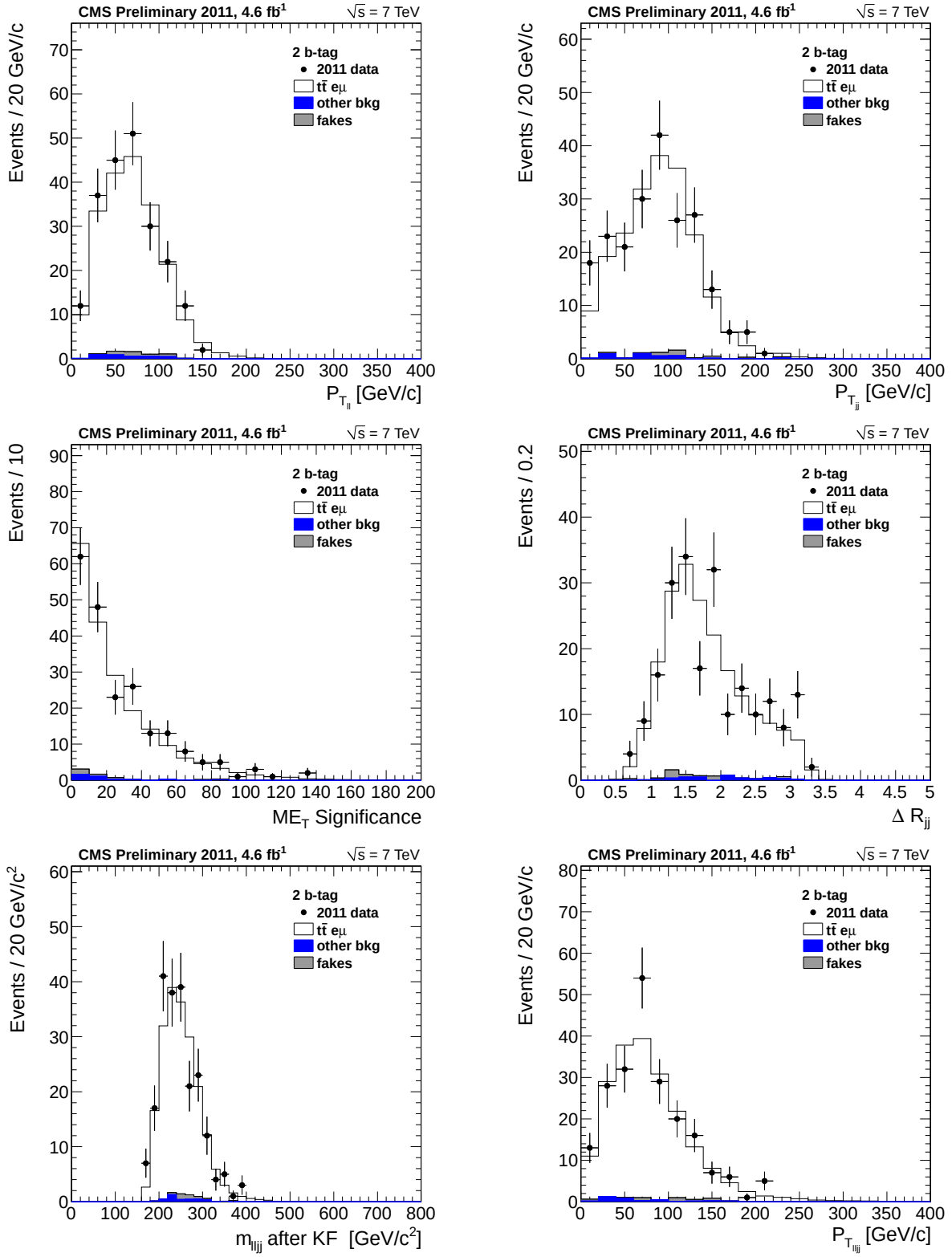

Figure 26: Comparison of 2011 $e\mu$ data to Powheg + Pythia top MC after two b-tag request, corresponding to an integrated luminosity of 4.6 fb^{-1}. Top: dilepton transverse momentum (left) and dijet transverse momentum (right). Center: missing transverse energy significance (left) and dijet ΔR_{jj} separation (right). Cuts described in the legend. Bottom: Dilepton + dijet "Higgs" invariant mass (left) and transverse momentum (right).

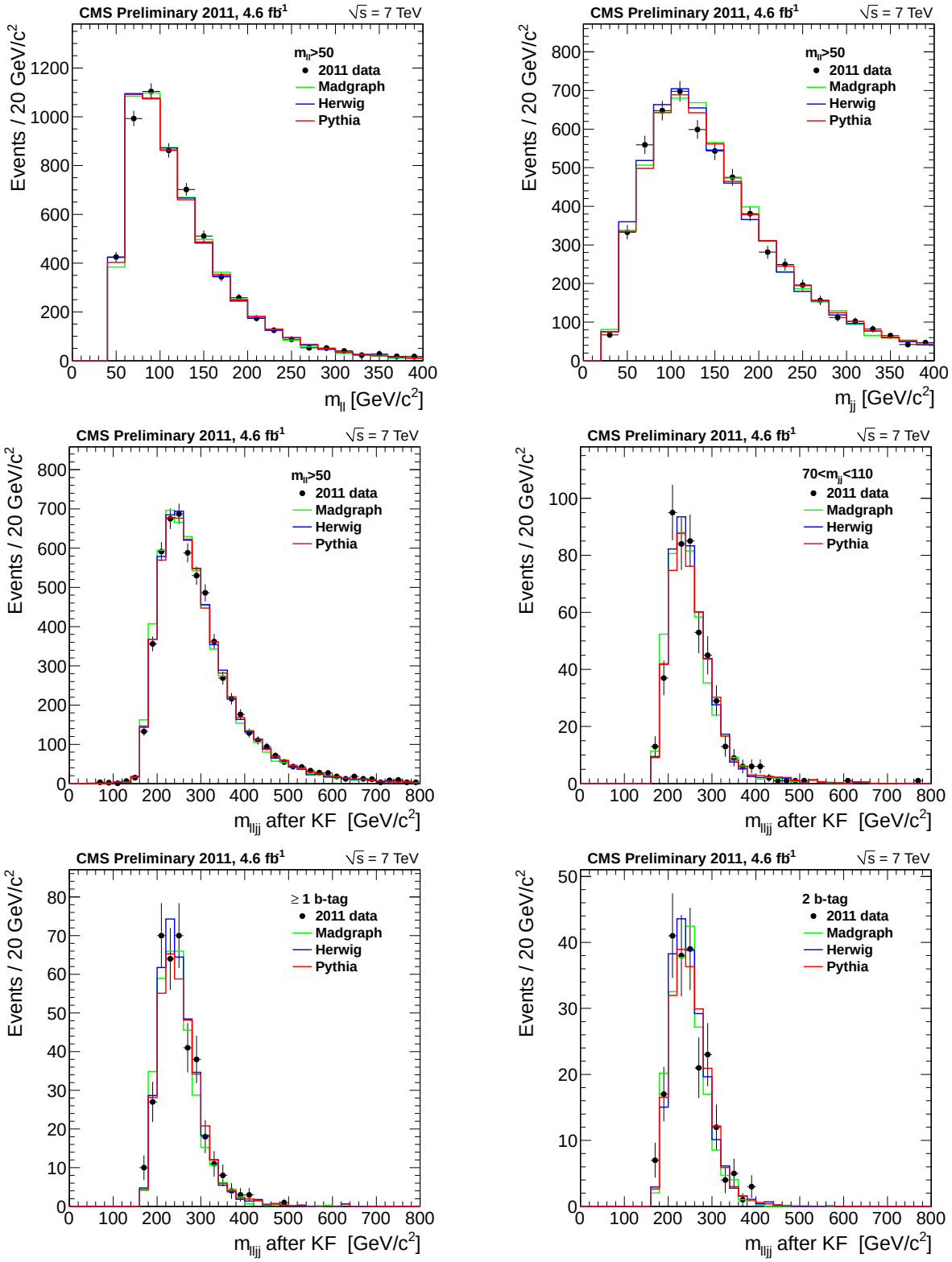

Figure 27: Shape comparison of 2011 $e\mu$ data to several Monte Carlos: inclusive Madgraph; di-lepton Powheg + Pythia; dilepton Powheg + Pythia. Top: di-jet (left) and di-lepton (right) mass. Center and bottom : di-jet + di-lepton"Higgs" candidate mass for several cuts, as described in the legends.

6 Correlated and Uncorrelated Systematic Uncertainties

Luminosity uncertainty has been estimated to be 6% [19, 20]. Sources of systematic uncertainties are the knowledge of lepton selection and b-tagging efficiency, the lepton and jets resolution and scales, the $\not{E}_T$ modeling, and knowledge of the signal and background shapes and cross sections.

Studies about jet resolution and efficiency, pile-up effects, and signal cross section uncertainties are described in Reference [21]. In the following subsections we describe lepton selection efficiencies, b-tagging, and background systematics.

6.1 b-tagging Systematics

A data-to-Monte Carlo scale factor (SF_b) has been measured for events containing b-jets as a function of p_T and η for the jets. This SF_b corrects for the more efficient identification of b-jets in Monte Carlo compared to data. Likewise, a mistag rate scale factor (SF_{mistag}) for light quarks misreconstructed as b-jets has been measured over a range of p_T and η for the jets. To study the systematic effects of b-tagging, both the SF_b and SF_{mistag} were simultaneously varied up and down by 10%.

The study was performed separately for the muon and electron channels, calculating the effect for signal MC.

Signal	2 Tags	1 Tag	0 Tags
Muons	$+13/-18\%$	3%	3-7%
Electrons	$+13/-18\%$	3%	3-7%

Table 11: b-tagging systematic uncertainty

Table 11 gives the b-tagging systematic uncertainty for the signal, for muons and electrons. The systematic effect is computed as the ratio of the number of tagged jets with a SF varied by plus and minus 10% to the number of tagged jets with the nominal SF. The uncertainty is reported for the cases where both jets are tagged, at least 1 jet is tagged, and no jets are tagged. In the analysis, the exact systematic uncertainty as a function of the Higgs mass is applied.

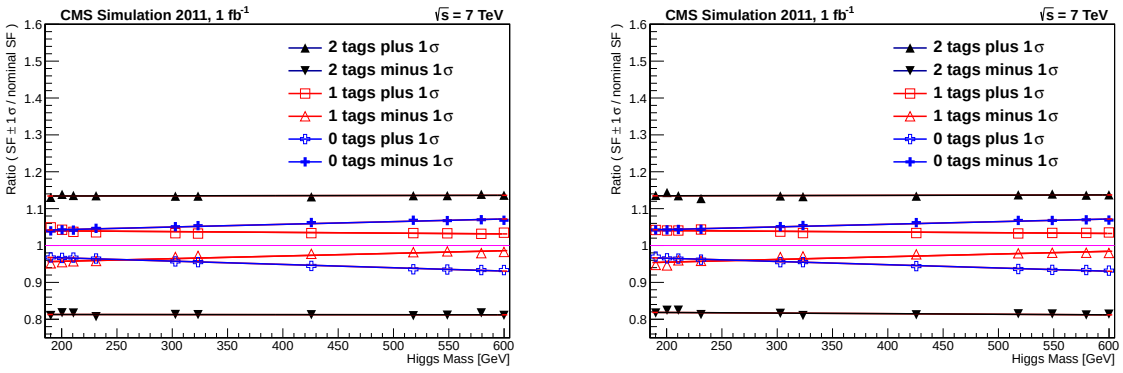

(a) Systematic uncertainty on the signal in the muon channel.

(b) Systematic uncertainty on the signal in the electron channel.

Figure 28: b-tagging systematic uncertainty for the signal in the muon and electron channel.

Figure 28 shows the b-tagging systematic uncertainty for the signal in the muon and electron

samples for the different cases of b-category where both jets are tagged, at least 1 jet is tagged, and no jets are tagged.

6.2 Leptons selection and Trigger efficiency

The efficiency of selecting a *lepton object* has been evaluated both on data 2011 and on simulation, selecting electron and muon objects closer as possible to the ones requested in the analysis from a single lepton trigger dataset. Therefore each event is required to contain at least two leptons belonging to Z decay and one jet, in order to match the analysis event topology.

The total efficiency measurement can be factorized into five sequential relative measurements. The five steps are: tracking efficiency, reconstruction efficiency, identification efficiency, isolation efficiency and the online or total trigger efficiency. The total is thus given by the product:

$$\epsilon_{lepton} = \epsilon_{tracking} * \epsilon_{RECO/Tracking} * \epsilon_{ID/RECO} * \epsilon_{ISO/ID} * \epsilon_{Trigger/ISO} \quad (1)$$

Each term is considered separately in the following and the values are provided by the official "tag-and-probe" method, a generic tool for measuring efficiencies using known resonances in p_T and η bins ($\epsilon_{tracking}$ is assumed to be very close to 100%) [22].

Given the intermediate p_T range ([20-100] GeV) of the lepton required for this analysis the Z resonance and its leptonic decay products are chosen to measure the efficiency with this method. It requires a mass constraint from a pair of same flavor lepton objects where on the two is tightly selected, the "tag", to ensure enough purity, and the other leg, the "probe" is used to measure efficiencies for a given identification criteria: efficiency is defined as the ratio of the number of probes passing the set of cuts to the total number of probes before the cuts.

Reconstruction and ID. Efficiencies computed for the lepton reconstruction and identification on data and simulation are evaluated as a function of the different η regions in a unique p_T range.

Tight cuts on the lepton Tag are requested, asking for a matching with the single trigger object and a very high reconstruction quality (VBTF) for both electrons and muons. For muons, identification criteria used for selecting the passing probes matches the ones of a VBTF muons with further requirements, like transverse and longitudinal impact parameter. For electrons the $\epsilon_{RECO/Tracking}$ is evaluated, meaning the efficiency of reconstructing an electron with *GSF* algorithm given the original super cluster in the calorimeter. Results are reported in Table 12. Instead, the electron identification efficiency is factorized together with isolation, by asking how many electrons having a WP95 (or WP80) are reconstructed, given a *GSF* electron, and values are reported in Table 13.

Isolation. Efficiencies for isolation have been computed requiring the passing probe to satisfy the criteria adopted for isolating leptons in this analysis. For the moment, the jet energy corrections due the pile-up are not taken into account in the definition of the isolation variable with respect to which the efficiency is computed, but studies have been demonstrated as changes are minor. Results are shown in Table 13. As explained, the electron identification efficiency is factorized together with isolation and a unique number is reported in the table, for the WP95.

Trigger. Concerning the trigger, efficiency that a lepton identified with the analysis criteria fired on the trigger used in the analysis has been evaluated. Using again the "tag-and-probe" method, a tight requirement on the tag is done, keeping the probe unbiased. More in detail the tag for muon is asked to be matched with the single trigger path, HLT_IsoMu24, being one of the lowest unprescaled trigger available in the menu. Then, probe is asked to geometrically

$\epsilon_{RECO} * \epsilon_{ID}$ for muons			
η coverage	p_T range (GeV)	Efficiency [%] (Data)	Data/MC ratio
$\lvert\eta\rvert < 1.20$	20-100	96.0 ± 0.1	0.996 ± 0.001
$1.20 < \lvert\eta\rvert < 2.40$	20-100	96.0 ± 0.1	0.986 ± 0.001
ϵ_{RECO} for electrons			
η coverage	p_T range (GeV)	Efficiency [%] (Data)	Data/MC ratio
$\lvert\eta\rvert < 0.80$	20-100	97.7 ± 0.3	0.999 ± 0.005
$0.80 < \lvert\eta\rvert < 1.44$	20-100	94.2 ± 0.3	0.964 ± 0.003
$1.44 < \lvert\eta\rvert < 1.57$	20-100	96.0 ± 0.6	0.99 ± 0.04
$1.57 < \lvert\eta\rvert < 2.0$	20-100	95.1 ± 0.5	0.992 ± 0.006
$2.0 < \lvert\eta\rvert < 2.5$	20-100	93.6 ± 0.4	1.001 ± 0.006

Table 12: *Reco/ID efficiency values from 2011 data and simulation using Tag and Probe method.*

ϵ_{ISO} for muons			
η coverage	p_T range (GeV)	Efficiency [%] (Data)	Data/MC ratio
$\lvert\eta\rvert < 0.9$	20-40	94.5 ± 0.5	0.987 ± 0.006
$0.9 < \lvert\eta\rvert < 2.4$	20-40	96.5 ± 0.4	0.995 ± 0.005
$\lvert\eta\rvert < 0.9$	40-100	98.7 ± 0.2	0.994 ± 0.002
$0.9 < \lvert\eta\rvert < 2.4$	40-100	99.2 ± 0.2	0.996 ± 0.002
$\epsilon_{ID} * \epsilon_{ISO}$ for electrons (WP95)			
η coverage	p_T range (GeV)	Efficiency [%] (Data)	Data/MC ratio
$\lvert\eta\rvert < 1.5$	20-40	91.6 ± 0.5	0.988 ± 0.006
$1.5 < \lvert\eta\rvert < 2.5$	20-40	83.1 ± 0.8	0.998 ± 0.011
$\lvert\eta\rvert < 1.5$	40-100	94.8 ± 0.2	0.988 ± 0.003
$1.5 < \lvert\eta\rvert < 2.5$	40-100	94.1 ± 0.3	1.016 ± 0.064

Table 13: *Isolation (together with identification, for electrons) efficiency values from 2011 data and simulation with Tag and Probe method.*

match with the offline trigger object and a value for the efficiency is extracted. Matching efficiency is of the order of permille, therefore negligible. For muons, the HLT_DoubleMu7 and

HLT_Mu13_Mu8 unprescaled trigger used in this analysis have been estimated on data. Since the HLT path is not simulated in the MC sample, the trigger is not applied on MC and this last is directly rescaled with the efficiency measured on data. The efficiency for this trigger have been found to vary as a function of η of the muon, therefore efficiencies for three distinct regions have been evaluated. In order to maximize the efficiency on the signal, the lowest unprescaled available single muon trigger, HLT_IsoMu24, has been used in the analysis as well. Here the efficiencies measured on data are lower than for the single leg of double trigger case, in particular for the outermost η region, likely due to tighter requirements on L1 quality level for the single trigger with respect to double. The efficiencies have been also evaluated in three different period, corresponding to the 2011 technical stops where, due to some changes at L1 seed, different values for the efficiencies are expected. Values are properly combined by weighting the final correction factor to be applied on MC event according to the integrated luminosity in where efficiencies are found be constant.
For the muon dataset the full 2011 data taking period A has been divided in 3 different periods in which the trigger conditions are found to be almost constants within them. They are reported in Table 14 together with the relative dataset used. Relative results are reported in Table 15, 16. For the single muon trigger a synoptic view of the results for the different periods is given in Table 17, while detailed results for different momentum and pseudorapidity ranges for each period are given in Figure 29. After May technical stop there are improvements due to changes at L1 in the CSCTF. A consistent drop in the efficiency is visible after EPS in the overlap and endcap regions.

Period	Dataset
before May TS (160404-163869)	/SingleMu/Run2011A-May10ReReco-v1
from May TS to EPS (165088-167913)	/SingleMu/Run2011A-PromptReco-v4
after EPS (167914-174752)	/SingleMu/Run2011A-Aug05ReReco-v1 + /SingleMu/Run2011A-PromptReco-v6

Table 14: Datasets used for Tag and Probe efficiency measurement

For electrons, efficiency for the HLT_Ele17Calo_Ele8Calo was measured on data to be greater than 99% for electrons with pT larger than 20 GeV through the entire ECAL fiducial region. More recently some new electron ID cuts have been applied to this path but efficiency is expected to be very close to 99%.

In order to properly take into account all the efficiencies, the single (ϵ_S) and the double trigger (ϵ_D) ones are combined according to the following formula to rescale the single MC event for a certain weight (w). This could be applied after being sure that both selected leptons from Z decay in the analysis have been matched with a trigger online object.

$$w = \epsilon_D(pt1,\eta1) * \epsilon_D(pt2,\eta2) + \epsilon_S(pt1,\eta1)(1-\epsilon_D(pt2,\eta2)) + \epsilon_S(pt2,\eta2)(1-\epsilon_D(pt1,\eta1)) \quad (2)$$

Trigger efficiencies were also evaluated for data corresponding to the so called 2011B period. For this period, unprescaled double muon (HLT_Mu13_Mu8 or HLT_Mu17_Mu8) and single muon (HLT_IsoMu24_eta2p1) triggers are used in the analysis. In the case of double muon trigger the results of the efficiency calculations for each single leg, as a function of p_T and η, are shown in Figure 30. Efficiency results for the single muon trigger are reported in Figure 31.

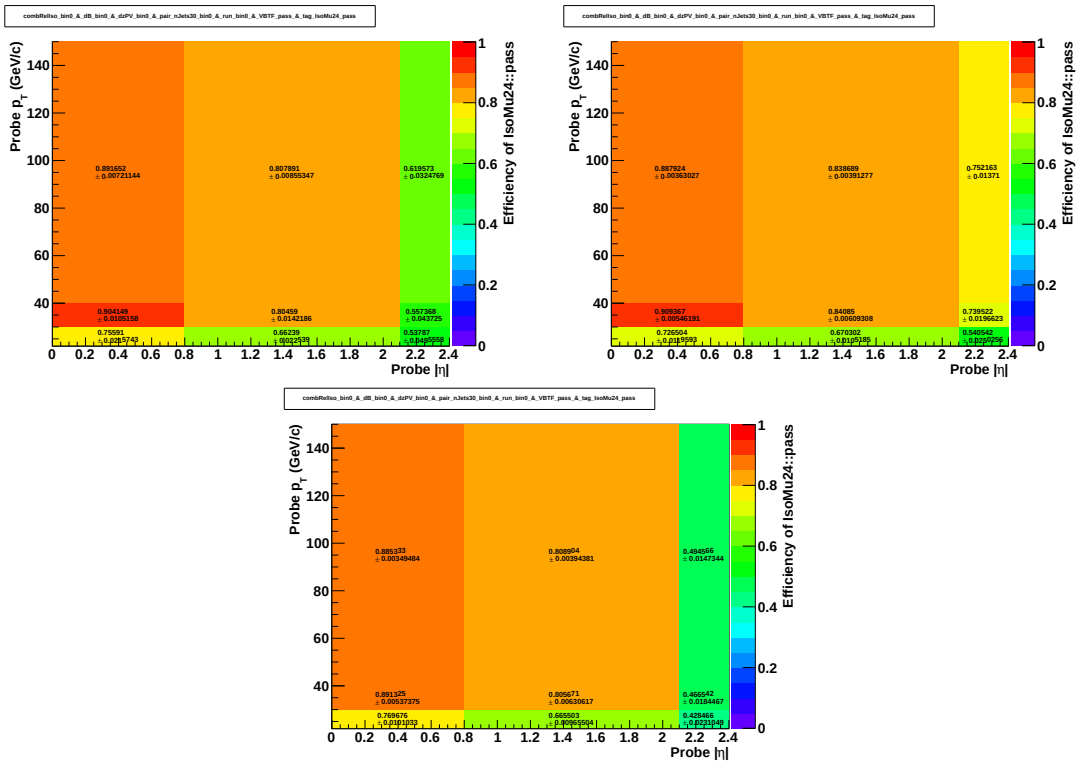

Figure 29: *Trigger efficiency values from 2011 data with Tag and Probe method for HLT_IsoMu24 in different period of data taking: upper-left is up to May TS, upper-right from MayTS up to EPS, while lower is for data taken between EPS and Aug TS.*

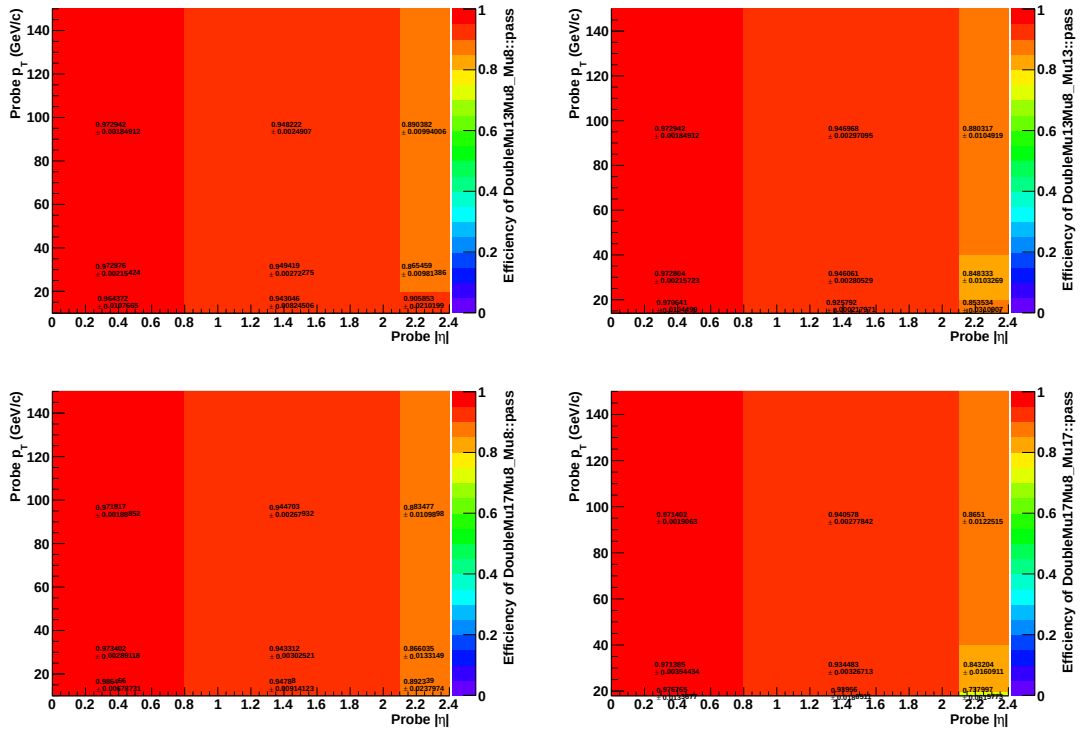

Figure 30: *Trigger efficiency values from 2011B data with Tag and Probe method for the singles legs of HLT_Mu13_Mu8 (upper row) and HLT_Mu17_Mu8 (lower row).*

$\epsilon_{Trigger}$ for HLT_DoubleMu7 (one leg)			
$p_T(GeV/c)$	$\|\eta\| < 0.8$	$0.8 < \|\eta\| < 2.1$	$2.1 < \|\eta\| < 2.4$
10-20	$97 \pm 2\%$	$95 \pm 1\%$	$96 \pm 3\%$
20-40	$97.5 \pm 0.4\%$	$95.0 \pm 0.6\%$	$92 \pm 1\%$
40-150	$97.3 \pm 0.4\%$	$94.6 \pm 0.5\%$	$91 \pm 1\%$

Table 15: *Trigger efficiency values from 2011 data with Tag and Probe method. Results for double muon trigger HLT_DoubleMu7 efficiency are reported according to different momentum and pseudorapidity range in which changes are expected*

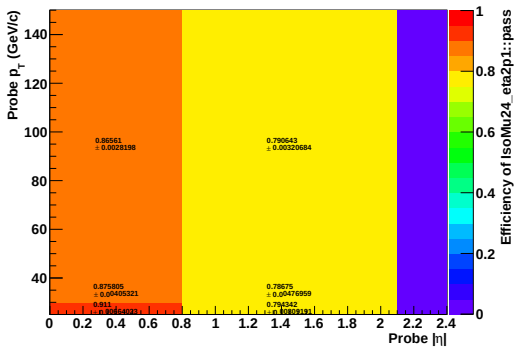

Figure 31: *Trigger efficiency values from 2011B data with Tag and Probe method for HLT_IsoMu24_eta2p1.*

$\epsilon_{Trigger}$ for HLT_Mu13_Mu8 (leg Mu13)			
$p_T(GeV/c)$	$\|\eta\| < 0.8$	$0.8 < \|\eta\| < 2.1$	$2.1 < \|\eta\| < 2.4$
10-20	$97.4 \pm 0.5\%$	$95.4 \pm 0.6\%$	$89 \pm 1\%$
20-40	$97.7 \pm 0.1\%$	$95.2 \pm 0.2\%$	$88.1 \pm 0.7\%$
40-150	$97.4 \pm 0.1\%$	$95.3 \pm 0.1\%$	$89.3 \pm 0.6\%$
$\epsilon_{Trigger}$ for HLT_Mu13_Mu8 (leg Mu8)			
10-20	$97.6 \pm 0.5\%$	$96.4 \pm 0.4\%$	$92 \pm 1\%$
20-40	$97.8 \pm 0.1\%$	$95.7 \pm 0.2\%$	$90.8 \pm 0.6\%$
40-150	$97.5 \pm 0.1\%$	$95.6 \pm 0.1\%$	$91.3 \pm 0.6\%$

Table 16: *Double trigger HLT_Mu13_Mu8 efficiency values from 2011 data and simulation with Tag and Probe method. In the upper(lower) table results for leg Mu13(Mu8) efficiency are reported: similar efficiencies for the two legs are found in particular in the central region .*

$\epsilon_{Trigger}$ for HLT_IsoMu24			
period (Integrated luminosity)	$\|\eta\| < 0.8$	$0.8 < \|\eta\| < 2.1$	$\|\eta\| > 2.1$
up to May TS (217 pb^{-1})	$89.6 \pm 0.1\%$	$80.7 \pm 0.1\%$	$60.8 \pm 0.1\%$
MayTS to EPS (920 pb^{-1})	$89.5 \pm 0.1\%$	$83.8 \pm 0.1\%$	$73.8 \pm 0.1\%$
EPS to Aug TS (219 pb^{-1})	$89.0 \pm 0.1\%$	$80.9 \pm 0.1\%$	$49.3 \pm 0.1\%$

Table 17: *Trigger efficiency values from 2011 data with Tag and Probe method. Results for the single muon trigger are reported, related to different periods in which changes are expected.*

6.3 Leptons energy scale and resolution

Systematic uncertainties can arise also from the lepton energy/momentum scale and resolution. Muon transverse momentum bias has been measured from 2010 data [23] as a function of the muon kinematic variables, and a clear dependence from the azimuthal angle of the muon was found. Nevertheless the maximum variation was found to be $\Delta p_T/p_T < 1\%$. For the electron energy scale variation of 2% for the central region and 5% for the endcap is applied. Numbers have been extracted from prompt reco, where laser corrections for the ECAL transparency were not yet applied. For a more consistent estimation the study will be repeated with re-reco sample.

6.4 Evaluation of systematic uncertainties

For each range a value for the ratio between efficiency on data and on simulation given by tag-and-probe method and the relative uncertainty is provided. The uncertainty on this ratio (σ_R) is computed by propagating single data and MC efficiency uncertainty. The final one considered includes:

$$\sigma_R^2 = \sigma_{stats+fit}^2 + \sigma_{syst}^2 \tag{3}$$

where σ_{syst} is intrinsic from tag and probe method (up to 0.4% for muons, 0.5% for electrons) and $\sigma_{stats+fit}$ is the statistical plus fit uncertainty. Each data/MC ratio has been used as correction factor to properly re-weight the MC events. In most of the cases the corrections factors to be applied have found to be larger than the calculated uncertainty on them. Therefore, in order to correctly evaluate the systematic uncertainty on the signal, the corrected MC has been varied by assigning $\pm\,\sigma_R$ of the uncertainty computed on the correction factor.

Then, using a cut and count approach, the variation of the final signal yields in the window $M_{Higgs} * 0.94 < M_{lljj} < M_{Higgs} * 1.1$ with respect to the corrected one, for different mass values, has been evaluated. No significative mass-dependence has been observed. The selection applied to compute the final yields is the one for 2b-tag category, but no variation is expected if considering the other categories, since the lepton selection cuts do not change.

The dielectron trigger is assumed to be fully efficient on data and therefore a 1% systematic is assigned to it.

Uncertainty on the muon momentum scale is propagated through the final yield by varying the muon p_T according to the function described in [23]. Same method has been adopted for quoting electron energy scale uncertainty. Final resulting values for the systematics are reported in Table 18.

category	$H \to ZZ \to \mu\mu jj$	$H \to ZZ \to ee\,jj$
Reco-ID-isolation	0.8%	3.4%
Trigger (HLT_Mu13_Mu8)	>2.0%	/
Trigger (HLT_IsoMu24)	>2.0%	/
Trigger (Ele17CaloEle8Calo)	/	1.0%
momentum/energy scale	1.0%	3.0%

Table 18: *Systematic uncertainties estimated for muon and for the electron channel.*

7 Signal Optimization

In order to increase the signal over background ratio in the analysis, we perform a signal optimization process taking as benchmark the object definitions described in section 3.1 and dividing the events in three tagging categories as described in section 3.2. A cut on the Z boson mass window, as expected from our signal, is applied by requiring $75 < m_{jj} < 105$ and $70 < m_{ll} < 110$. An extra cut on MET significance smaller than 10, described in section 3.3, is also applied in the double tagged region.

On top of the previous selection, two different techniques are explored to separate signal and background taking advantage of the angular distribution information of the final objects. Signal optimization proccesses based on a Likelihood Discriminant and a Neural Network are described in the following sections.

7.1 Signal Optimization Based on Helicity Likelihood Discriminant

The angular optimization is based on the LD introduced in section 3.4. We select events with a LD value greater than 0.5 in the 2tag category.

We check the performance of the analysis applying the described optimization to MC simulation normalized to the luminosities in 2011A (2.1 fb^{-1}) and 2011B (1.8 fb^{-1}) data.

The m_{jjll} distribution in the final region is shown in Figures 32. Cutting on different mass ranges we obtain different optimizations as a function of the Higgs mass, as shown in Tables 19 and 20 for electrons and muons in 2011A data.

The same set of plots and tables are shown for 2011B data (Fig. 33, Tables 21 and 22).

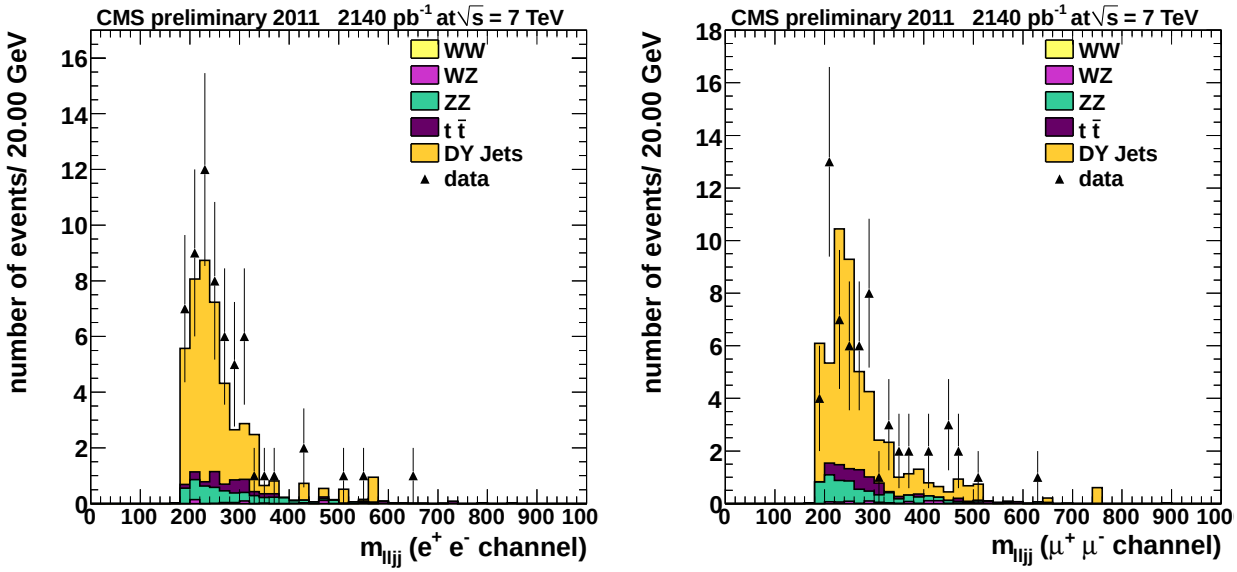

Figure 32: Distribution of the m_{jjll} for electron (left) and muon (right) events in 2.1 fb^{-1} of 2011A data. Higgs signal with a mass of 500 GeV is shown in orange, stacked on top of the SM backgrounds.

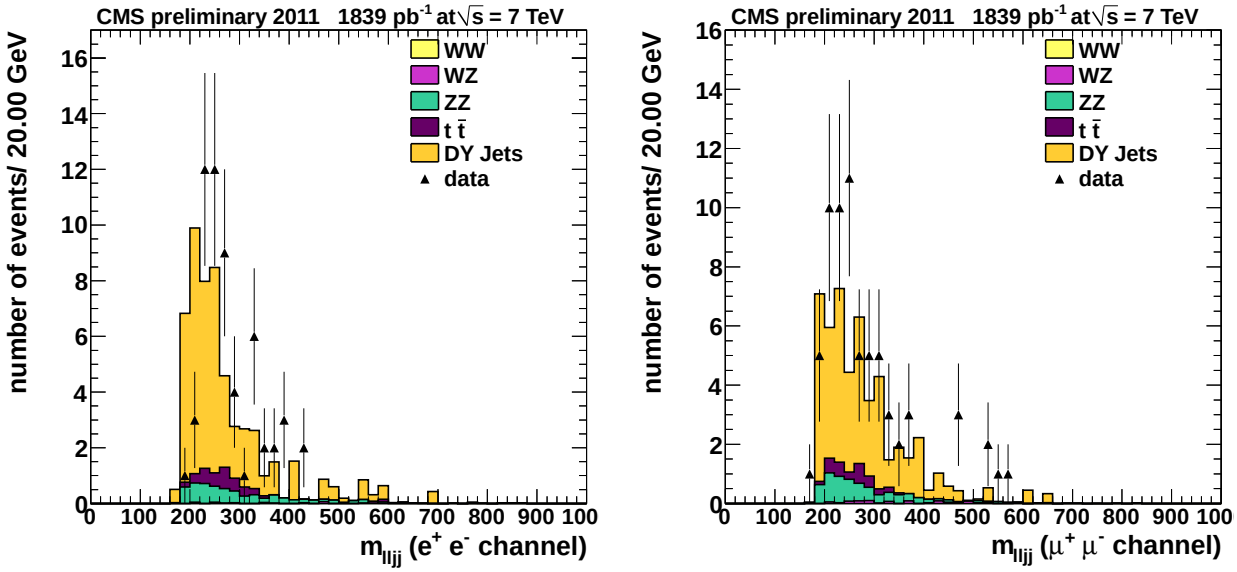

Figure 33: Distribution of the m_{jjll} for electron (left) and muon (right) events in 1.8 fb^{-1} of 2011B data. Higgs signal with a mass of 500 GeV is shown in orange, stacked on top of the SM backgrounds.

Process	Electrons						
Mass Range	Total	[235,275]	[282,330]	[329,385]	[376,440]	[423,495]	[470,550]
Z+Jets	38.6	11.3	4.6	1.8	0.7	0.3	0.6
$t\bar{t}$	2.8	0.7	1.1	0.2	0.0	0.1	0.0
ZZ	5.2	1.1	0.8	0.6	0.4	0.3	0.2
WZ	0.6	0.0	0.1	0.1	0.0	0.1	0.1
WW	0	0	0	0	0	0	0
Total Bkg	47.2	13.1	6.6	2.7	1.1	0.8	0.9
Data	61	15	12	2	2	2	2
Signal	-	2.4	3.0	3.3	2.5	1.6	1.1

Table 19: Number of electron events expected in the final region and splitted in different Higgs mass ranges. 2011A data (2.1 fb^{-1}).

Process	Muons						
Mass Range	Total	[235,275]	[282,330]	[329,385]	[376,440]	[423,495]	[470,550]
Z+Jets	42.9	13.2	5.2	2.7	2.4	2.1	1.2
$t\bar{t}$	3.6	1.02	0.9	0.1	0.1	0.1	0.1
ZZ	6.5	1.4	0.9	0.6	0.6	0.3	0.2
WZ	1.0	0.1	0.1	0.1	0.2	0.2	0.2
WW	0	0	0	0	0	0	0
Total Bkg	54.0	15.7	7.1	3.5	3.3	2.7	1.7
Data	61	11	10	6	2	5	3
Signal	-	2.6	3.1	3.6	3.0	1.8	1.2

Table 20: Number of muon events expected in the final region and splitted in different Higgs mass ranges. 2011A data (2.1 fb^{-1}).

Process	Electrons						
Mass Range	Total	[235,275]	[282,330]	[329,385]	[376,440]	[423,495]	[470,550]
Z+Jets	45.3	10.5	4.7	3.2	1.9	1.2	1.3
$t\bar{t}$	3.5	1.2	0.8	0.2	0.0	0.0	0.0
ZZ	5.9	1.2	0.8	0.6	0.5	0.4	0.3
WZ	0.3	0.1	0.1	0.1	0.1	0.1	0.1
WW	0	0	0	0	0	0	0
Total Bkg	55.0	13.0	6.4	4.1	2.5	1.7	1.7
Data	57	19	8	7	5	0	0
Signal	-	2.6	3.1	3.5	2.8	1.6	1.1

Table 21: Number of electron events expected in the final region and splitted in different Higgs mass ranges. 2011B data (1.8 fb^{-1}).

Process	Muons						
Mass Range	Total	[235,275]	[282,330]	[329,385]	[376,440]	[423,495]	[470,550]
Z+Jets	40.3	9.4	7.2	2.8	3.8	1.3	0.5
$t\bar{t}$	2.8	1.1	0.7	0.1	0.0	0.0	0.0
ZZ	6.3	1.5	0.8	0.8	0.4	0.2	0.2
WZ	0.8	0.1	0.1	0.1	0.1	0.2	0.2
WW	0	0	0	0	0	0	0
Total Bkg	50.2	12.1	8.8	3.8	4.3	1.7	0.9
Data	67	19	10	7	2	3	2
Signal	-	2.7	2.9	3.8	2.8	1.7	1.1

Table 22: Number of muon events expected in the final region and splitted in different Higgs mass ranges. 2011B data (1.8 fb^{-1}).

7.2 Signal Optimization Based on Helicity Neural Network

A Neural Network is applied to separate Higgs signal from background using the five helicity angles of the final objects in the analysis as inputs. A training and test evaluation has been performed with the framework of the TMVA package [24] using the real mixture of MC processes as background and Higgs MC. Both the training and testing samples for both background and signal are constructed and events randomly mixed outside of the Neural Network. There are 37,874 signal events and 38,378 background events evenly split between testing and training. The Neural Network was trained on the Monte Carlo generated for a hypothetical Higgs mass of 400 GeV/c^2. This training was on events that passed the previously explained preselection, the Z boson mass window cuts previously explained, but before the cut on MET significance.

7.2.1 Neural Network Architecture

The architecture of the Neural Network consists of two hidden layers with N and N neurons respectively, where N is the number of variables, and one output node as shown in Figure 34.

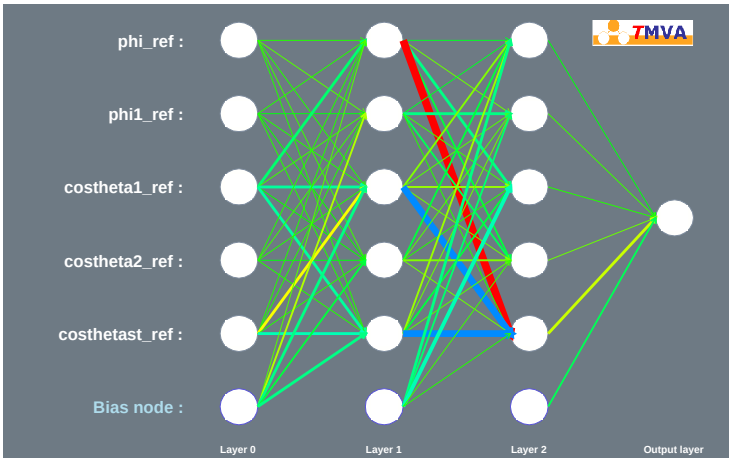

Figure 34: Neural Network architecture used for the training.

7.2.2 Input Variables and Training

The input variables for the Neural Network are the same variables that are used for the Helicity Likelihood Discriminant, phi, phi1, costheta1, costheta2, and costhetastar. The input variable distributions for both signal and background are shown in Figure 35. The default values are used when booking the Multi Layer Perceptron Neural Network except for the Hidden Layers as described in the previous subsection, and the number of cycles which is set to 1000. The background rejection versus signal efficiency for the input signal and background is shown in Figure 36.

7.2.3 Results Based on Helicity Neural Network

The training and testing of the Neural Network can bee seen in Figure 37. While there is separation between the signal and background, and good agreement between testing and training, there is a spike in background at the same place as the signal, and the Neural Network output does not continue to 1. The training was done with Monte Carlo generated for a hypothetical Higgs mass of 400 GeV but then applied to the Monte Carlo for hypothetical Higgs masses of 200, 300, 400, and 500 GeV. This is because the angular components should not depend on Higgs mass.

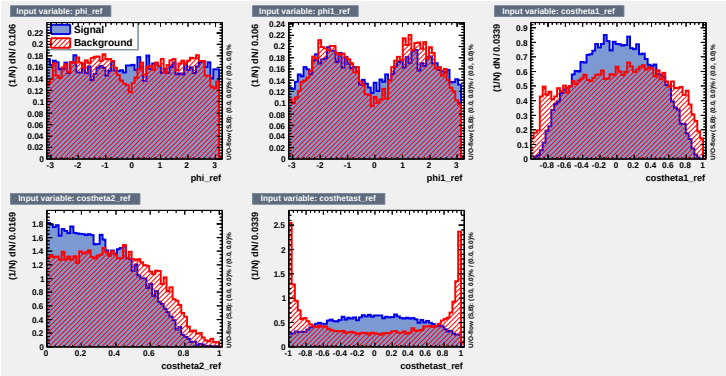

Figure 35: Signal and Background for the the Input Variables for the Neural Network training.

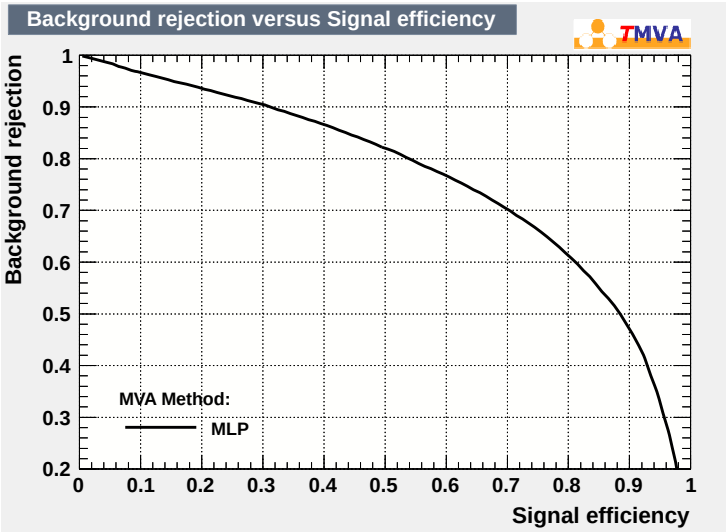

Figure 36: Background Rejection Versus Signal Efficiency for the input and output of the Neural Network.

In the 1tag region after applying the additional MET significance cut the separation between signal and background looks similar to the training for Higgs 300, 400, and 500 GeV, but does not have much discrimination power for a Higgs of 200 GeV. The discrimination power is virtually the same after applying an additional cut of of -6%/+10% of the Higgs mass for all four cases as seen in Figure 38. When comparing background rejection versus signal efficiency between the Neural Network and Likelihood Discriminate the performance is for all practical purposes the same. See Figure 40.

In the 2tag region after applying the additional MET significance cut and a cut of of -6%/+10% of the Higgs mass, the discriminating power of the Neural Network is similar to the 1tag case with poor ability for a Higgs of 200 GeV, but good seperation for Higgs of 300, 400, and 500 GeV. This is shown in Figure 39. When comparing background rejection versus signal efficiency between the Neural Network and Likelihood Discriminate the performance is roughly the same, except for the Higgs of 200 GeV case where the Neural Network is almost consistantly better than the Likelihood Discriminate. This is shown in Figure 41.

With the Neural Network performing so close to the Helicity Likelihood Descriminate there are

a nummber of prommising ways that this analysis might be improved. Adding additional information into the training like the MET significance variable, or other variables could improve performance. Also a closer look at at the network archetecture which was arbitrarily chosen in this case may provide better descriminating power. Training on just events that have at least one btag or only in the 2tag region may also prove useful. From this initial look, using a Neural Network on this channel shows promise.

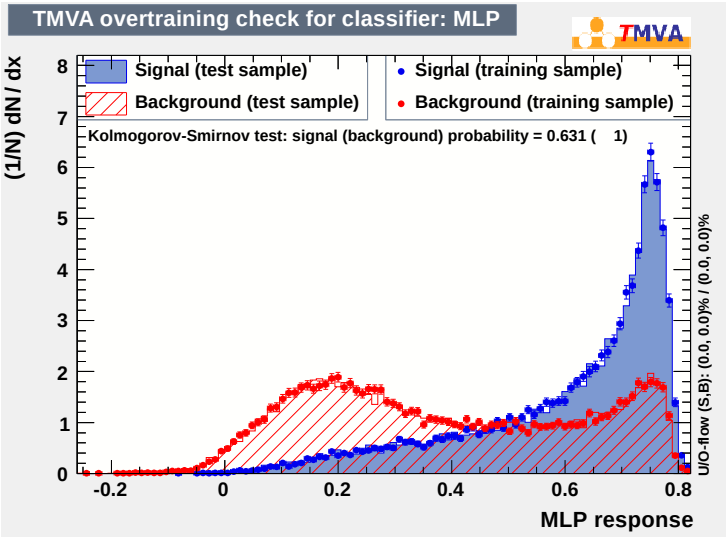

Figure 37: Signal and Background output for both the testing and training of the Neural Network output.

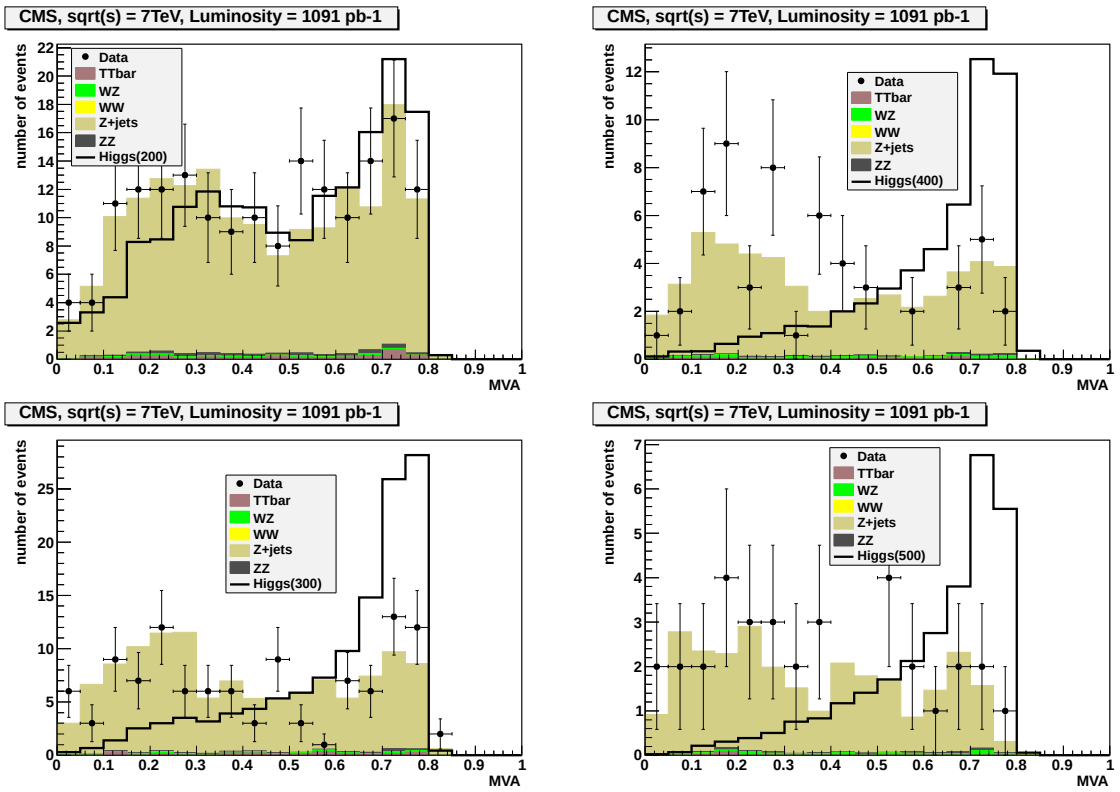

Figure 38: Signal and background Neural Network output in the 1tag region after preselection, the Z boson mass window cuts, cut on MET significance, and a -6%/+10% Higgs mass window. The signal is scaled to the sum of the Monte Carlo background.

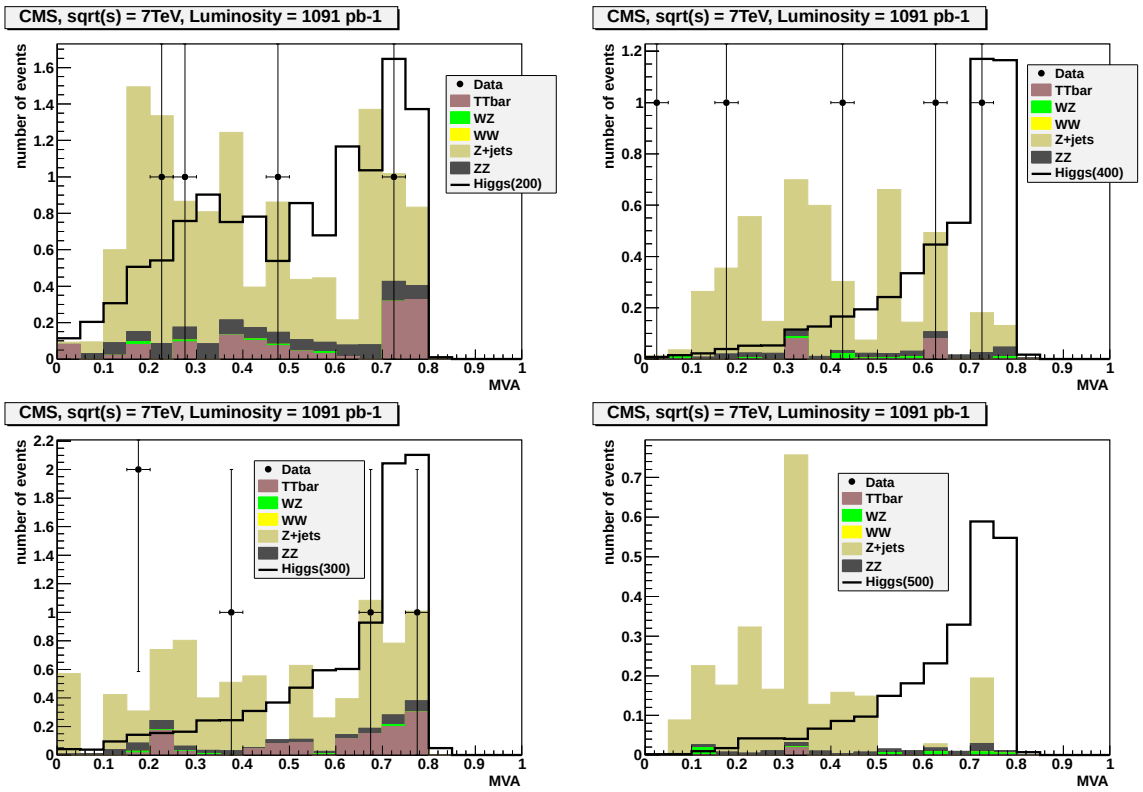

Figure 39: Signal and background Neural Network output in the 2 tag region after preselection, the Z boson mass window cuts, cut on MET significance, and a -6%/+10% Higgs mass window. The signal is scaled to the sum of the Monte Carlo background.

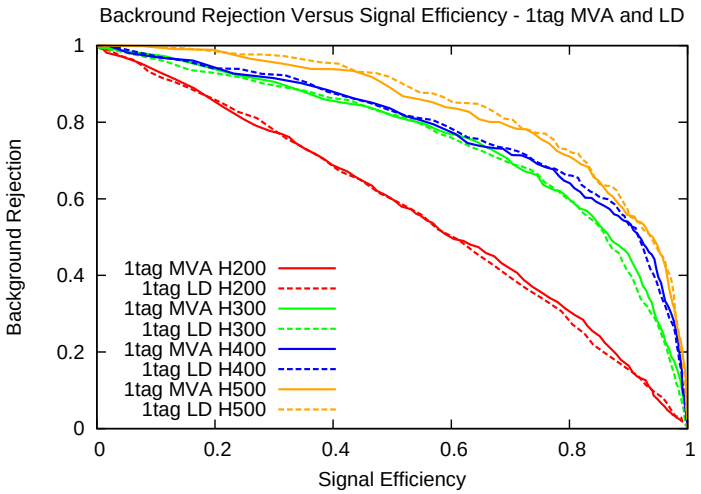

Figure 40: Background Rejection Versus Signal Efficiency in the 1tag region comparing the Multi Variant Analysis output to the the Helicity Likelihood Discriminant for a Higgs mass of 200, 300, 400, and 500 GeV. This is calculated after preselection cuts, Z boson mass cuts, cut on MET significance, in a -6%/+10% Higgs mass window.

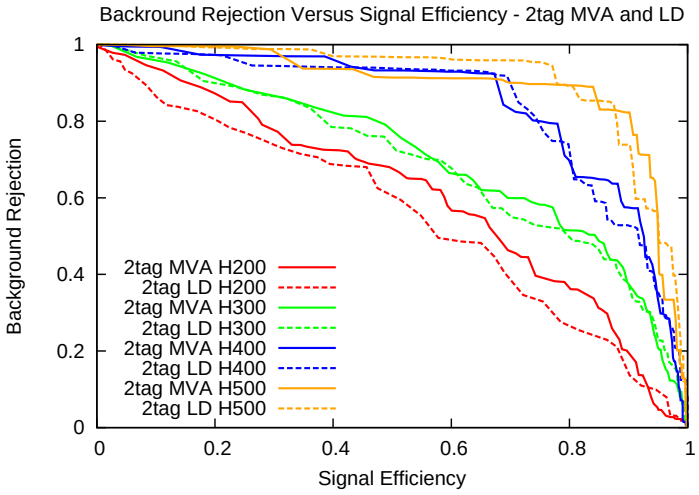

Figure 41: Background Rejection Versus Signal Efficiency in the 2tag region comparing the Multi Variant Analysis output to the the Helicity Likelihood Discriminant for a Higgs mass of 200, 300, 400, and 500 GeV. This is calculated after preselection cuts, Z boson mass cuts, cut on MET significance, in a -6%/+10% Higgs mass window.

8 Statistical Analysis and Results

We determine the expected upper limits to the Standard Model Higgs production cross section as a function of the Higgs boson mass assuming as reference an integrated luminosity of 1 fb^{-1}. We use the official tool developed by the CMS Higgs combination group [25] that supports different methods, including Bayesian approach, frequentist profile likelihood, and Feldman-Cousins [26] methods, and the modified frequentist CLs method [27] with Cousins-Highland integration of nuisance parameters for the treatment of systematic uncertainties [28]. The tool uses the `RooStats` [29] engine from ROOT as internal implementation. We determine the expected upper limit to the Higgs boson production cross section times branching fraction to $\ell\ell b\bar{b}$. The limit is expressed as ratio r of the determined upper limit to the cross section times branching ratio divided by its standard model expectation. A value of the Higgs boson mass m_H is excluded if, for that mass hypothesis, r is less than one.

There are two main possible general approaches to determine the limit to the Higgs cross sections.

The simples approach, referred to as "cut and count" analysis, uses only the number of events selected within a given window in the reconstructed Higgs mass, $m_{\ell\ell jj}$, around an assumed value m_H of the Higgs boson mass. The Higgs cross section limit is determined from the expected number of signal and background events passing the selections s and b respectively. We combine using Poissonian statistics the counting information from the two channels with electrons and muons. The sources of systematic uncertainties on s and b are taken into account in the determination of the limit assuming log-normal distributions of the nuisance parameters.

Another possible approach, referred to as "shape analysis", takes into account the measured distribution of variables that can discriminate Higgs signal events against background events. In the case of the $H \to ZZ \to \ell^+\ell^- b\bar{b}$ analysis, the main discriminant variable is the reconstructed Higgs boson mass, $m_{\ell\ell jj}$, which is peaked around the true Higgs boson mass, m_H, for the signal and has a broader distribution for background processes. We can develop an analysis that does not select signal events cutting on $m_{\ell\ell jj}$, and we can use the distribution of $m_{\ell\ell jj}$ for selected events, comparing to the expected distribution from signal and background. The possible sources of systematic uncertainties on both the expected signal and background yields and the shape of signal and background distributions are considered in the limit extraction procedure. The shape analysis can be implemented in the Higgs combination tool using an unbinned approach with an extended likelihood function defined by:

$$-\ln \mathcal{L} = \sum_{j=1}^{k} \left[s_j + b_j - \sum_{i=1}^{n_j} \left(s_j \mathcal{P}_s^{(j)}(m_i^{(j)}) + b_j \mathcal{P}_b^{(j)}(m_i^{(j)}) \right) \right] , \tag{4}$$

where k is the number of channels (in our case $k = 2$, and $j = 1, 2$ correspond to the electon and muon channels), n_j is the number of selected candidate events in the channel j, s_j and b_j are the expected signal and background events, $\mathcal{P}_s^{(j)}$ and $\mathcal{P}_b^{(j)}$ are the probability density functions for signal and background, and $m_i^{(j)}$ are the n_j values of $m_{\ell\ell jj}$ of the selected candidates in the channel j. As alternative, the distribution of $m_{\ell\ell jj}$ can be sub-divided into bins, and in that cases the number of selected events in each bin is considered with the corresponding expected number of events from signal and background in that bin, and the information from all bins is combined using a Poissonian likelihood, similarly to the "cut and count" case, but with more channels.

Results combining all the H→ZZ→ 2ℓ2q categories (with and without tagging) are described

in Reference [17].

9 Conclusions

We present a search for a Standard Model Higgs boson decay to two Z bosons with a subsequent decay to a semileptonic final state with two leptons and two b-jets, $H \to ZZ \to 2l2b$.

We performed an optimization of the selection cuts based on kinematic and topological quantities. A study of systematics errors have been done focusing mainly on lepton selection efficiency and b-tagging. Full analysis is validated using 4 fb^{-1} data collected in 2011.

References

[1] G. Abbiendi et al., The ALEPH, DELPHI, L3 and OPAL Collaborations, The LEP Working Group for Higgs Boson Searches, "Search for the Standard Model Higgs Boson at LEP", *Phys. Lett* **B565** (2003) 61–75. doi:10.1016/S0370-2693(03)00614-2.

[2] T. Aaltonen et al, The CDF and D0 Collaborations, "Combination of Tevatron searches for the standard model Higgs boson in the W+W- decay mode", *Phys. Rev. Lett.* **104** (2010) 061802. doi:10.1103/PhysRevLett.104.061802.

[3] T. Aaltonen et al, The CDF, D0 Collaborations, the TEVNPHWG Working Group, "Combined CDF and D0 Upper Limits on Standard Model Higgs Boson Production with up to 8.2 fb-1 of Data", *FERMILAB-CONF-11-044-E* (2011) arXiv:1103.3233.

[4] The ALEPH, CDF, D0, DELPHI, L3, OPAL, SLD Collaborations, the LEP Electroweak Working Group, the Tevatron Electroweak Working Group, and the SLD electroweak and heavy flavour groups, "Precision Electroweak Measurements and Constraints on the Standard Model", *LEPEWWG* **2010-01** (2010) arXiv:1012.2367.

[5] J. Alwall, P. Demin, S. de Visscher et al., "MadGraph/MadEvent v4: the new web generation", *JHEP* **09** (2007) 028, arXiv:0706.2334. doi:10.1088/1126-6708/2007/09/028.

[6] P. Nason, "A New Method for Combining NLO QCD with Shower Monte Carlo Algorithms", *JHEP* **11** (2004) 040. doi:10.1088/1126-6708/2004/11/040. arXiv:hep-ph/0409146.

[7] S. Frixione, P. Nason, and C. Oleari, "Matching NLO QCD Computations with Parton Shower Simulations: the POWHEG method", *JHEP* **11** (2007) 070. doi:10.1088/1126-6708/2007/11/070. arXiv:0709.2092.

[8] S. Alioli, P. Nason, C. Oleari et al., "NLO Vector-Boson Production Matched with Shower in POWHEG", *JHEP* **07** (2008) 06. doi:10.1088/1126-6708/2008/07/060. arXiv:0805.4802.

[9] LHC Higgs Cross Section Working Group, S. Dittmaier, C. Mariotti et al., "Handbook of LHC Higgs Cross Sections: 1. Inclusive Observables", *CERN-2011-002* (CERN, Geneva, 2011) arXiv:1101.0593.

[10] CMS Collaboration, "Performance of CMS muon identification in pp collisions at $\sqrt{s} = 7$ TeV", *CMS PAS* **MUO-2010-002** (2010).

[11] CMS Collaboration, "Electron Reconstruction and Identification at $\sqrt{s} = 7$ TeV", *CMS Detector Performance Summary* **DP-2010-032** (2010).

[12] CMS Collaboration, "Particle-flow commissioning with muons and electrons from J/Psi, and W events at 7 TeV", *CMS PAS* **PFT-2010-003** (2010).

[13] M. Cacciari, G. P. Salam, and G. Soyez, "The anti-k_t jet clustering algorithm ", *JHEP* **04** (2008) 063. doi:10.1088/1126-6708/2008/04/063.

[14] A. Rizzi, F. Palla, and G. Segneri, "Track impact parameter based b-tagging with CMS", *CMS Note* **CMS-AN-2006/019** (2006).

[15] CMS Collaboration, "Performance of b-jet identification in CMS", *CMS Physics Analysis Summary* **CMS-PAS-BTV-11-001** (2011).

[16] M. Segala, K. Gennadiy, and M. Meenakshi, "Measurement of b-tagging efficiency in semi-leptonic decays of $t\bar{t}$ events using the Flavor-tag Consistency Method", *CMS Note* **CMS-AN-2011/183** (2011).

[17] S. Bolognesi, A. Bonato, D. Del Re et al., "Search for the standard model Higgs Boson in the decay channel $H \to ZZ \to 2\ell 2q$ at CMS", *CMS Note* **CMS-AN-2011/388** (2011).

[18] T. Gleisbergand et al., "Event generation with SHERPA 1.1",. doi:10.1088/1126-6708/2009/02/007. arxiv: 0811.4622.

[19] CMS Collaboration, "Measurement of CMS luminosity", *CMS PAS* **EWK-2010-004** (2010).

[20] CMS Collaboration, "Absolute luminosity normalization", *CMS DPS* **2011-002** (2011).

[21] S. Bolognesi, A. Bonato, A. D. Del Re, A.and Gritsan et al., "Search for a Semileptonic Decay of a SM Higgs or BSM Boson $H \to ZZ \to 2l2j$", *CMS Note* **CMS-AN-2011/100** (2011).

[22] C. Collaboration, "Measurements of InclusiveWand Z Cross Sections in pp Collisions at $\sqrt{s}$ = 7 TeV", *JHEP* **1101** (2011) 080. doi:10.1007/JHEP01(2011)080.

[23] CMS Collaboration Collaboration, "Performance of muon reconstruction and identification in pp collisions at $\sqrt{s}$=7 TeV", *CMS PAS* **CMS-MUO-10-004under approval** (2010).

[24] A. Hocker et al. arXiv:0703039.

[25] C. H. C. Group, "Documentation of the RooStats-based statistics tools for Higgs PAG", *CMS TWiki* SWGuideHiggsAnalysisCombinedLimit (2011).

[26] G. J. Feldman and R. D. Cousins, "Unified approach to the classical statistical analysis of small signals", *Phys. Rev* **D 57** (1998) 3873–3889. doi:10.1103/PhysRevD.57.3873.

[27] A. L. Read, "Modified Frequentist Analysis of Search Results (The CLs Method)", *CERN OPEN* **2000-205** (2000).

[28] R. D. Cousins and V. L. Highland, "Incorporating systematic uncertainties into an upper limit", *Nucl. Instr. Meth* **A 320** (1992) 331–335. doi:doi:10.1016/0168-9002(92)90794-5.

[29] L. Moneta, K. Belasco, K. Cranmer et al., "The RooStats Project", *PoS* **ACAT2010** (2010) 057. [arxiv:1009.1003].

A B-tagging optimization

Six different cases for defining b-tag categories were studied for the Track Counting High Efficiency (TCHE) and Track Counting High Purity (TCHP) B-taggers. For each case, the 95% C.L. upper limit on expected $\sigma \times$ BR for the process $H \to ZZ \to \ell\ell + 2$jets was computed. In order to arrive at the optimal choice of the b-tag category and the algorithm, the one which led to the lowest 95% C.L. upper limit on the $\sigma \times$ BR was chosen.

We determined which B-tagging algorithm gives the lowest value for the upper 95% expected limit on the ratio of the number of signal events to the number of expected signal events. For each case the event was categorized to have two, one or zero tagged jets by checking if the jets passed or failed a series of discriminating values for the given b-tagging algorithm. If both the jets passed the tagging requirements the event was considered to have two tagged jets. If this failed, we checked whether there was exactly one jet that passed the tagging requirement; in this case, the event was categorized as one tagged jet event. If this also failed, the event was considered to have zero tagged jets. The list below describes the six cases which were considered for each algorithm.

- Case 1: 2 jets pass loose, 1 jet passes loose, No jets pass
- Case 2: 2 jets pass loose, 1 jet passes medium, No jets pass
- Case 3: 1 jet passes loose and 1 jet passes medium, 1 jet passes loose, No jets pass
- Case 4: 1 jet passes loose and 1 jet passes medium, 1 jet passes medium, No jets pass
- Case 5: 2 jets pass medium, 1 jet passes loose, No jets pass
- Case 6: 2 jets pass medium, 1 jet passes medium, No jets pass

	Loose	Medium
TCHE	1.7	3.3
TCHP	1.19	1.93

Table 23: Loose and medium working points for the Track Counting High Efficiency and Track Counting High Purity B-tagging algorithms

In the list above “loose“ and “medium“ refer to the loose and medium working points for each algorithm, their values can be found in Table 23.

Figure 42 shows the 95 % C.L. upper limit on expected $\sigma \times$ BR for the process $H \to ZZ \to \ell\ell +$ 2jets for each tagging case and for various masses of the Higgs Boson. Although a single case does not always gives the lowest upper limit, on average case 3 for the Track Counting High Efficiency gives the best overall results and should thus be used for the tagging requirement.

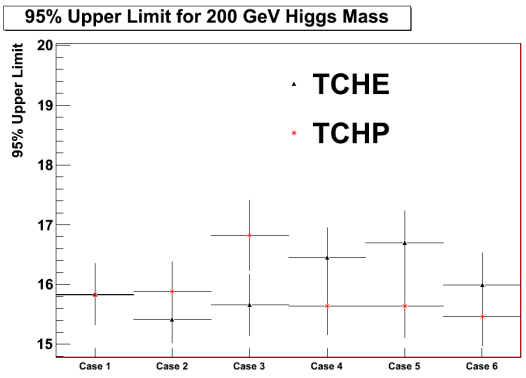

(a) 200 GeV Higgs Mass

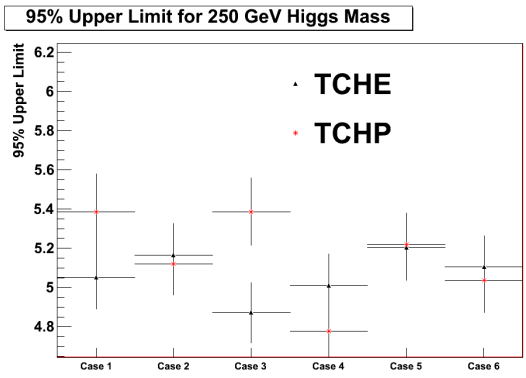

(b) 250 GeV Higgs Mass

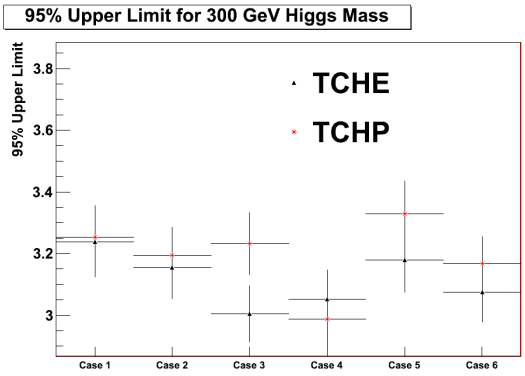

(c) 300 GeV Higgs Mass

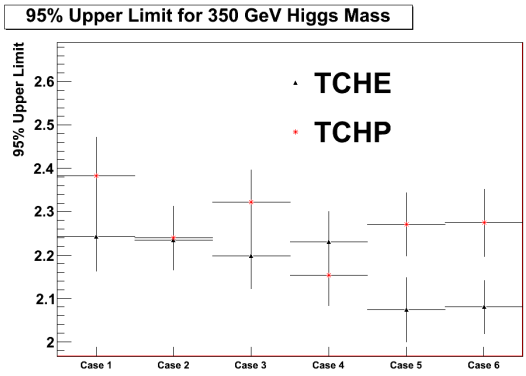

(d) 350 GeV Higgs Mass

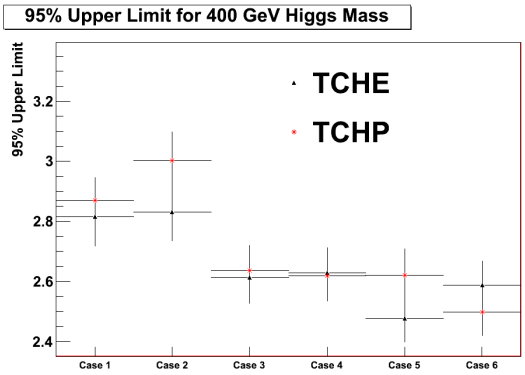

(e) 400 GeV Higgs Mass

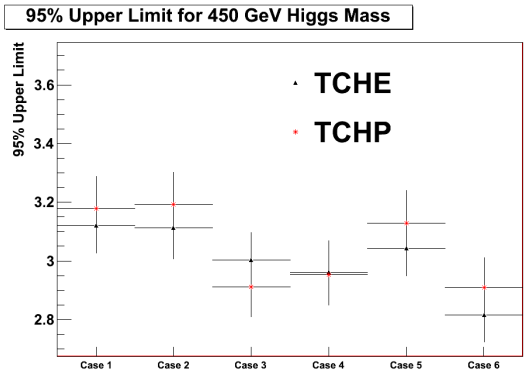

(f) 450 GeV Higgs Mass

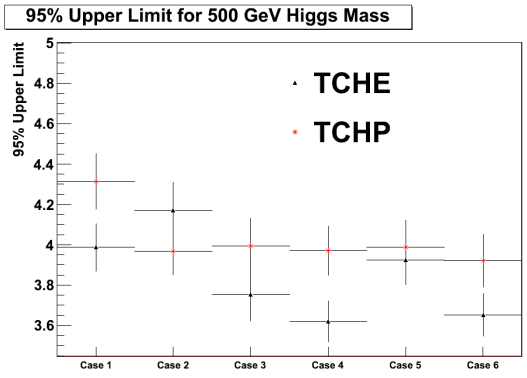

(g) 500 GeV Higgs Mass

Figure 42: 95 % upper Limit for each Higgs Mass. Each plot shows how the tagging algorithms perform for each case.

B Check of the CSV tagger in the analysis regions

The Combined Secondary Vertex (CSV) tagger was studied in the final regions of the analysis comparing its performance with the TCHE tagger. The inclusive distribution of the CSV tagger discriminator, comparing data and MC, is shown in Figures 43 and 44 for muon and electron events. The discriminator is shown separately for leading and second leading jets.

The number of observed and expected events were checked in the one and two-tag final regions using the TCHE and CSV taggers. In both cases, no major differences were observed. The overall behavior is stable, in particular for the backgrounds were real b-jets are expected like the $t\bar{t}$ production. For the $Z + jets$ background, an small increase of tagged events was found using the CSV tagger. This increase is due to the fact that the CSV has a bigger mistag rate in this particular sample.

A detailed comparison is shown in Table 24 for the one-tag region, and in Table 24 for the two-tag region.

For the 2011 round of the analysis no changes on the tagging algorithm will be applied, therefore the TCHE tagging algorithm will remain as the selected one.

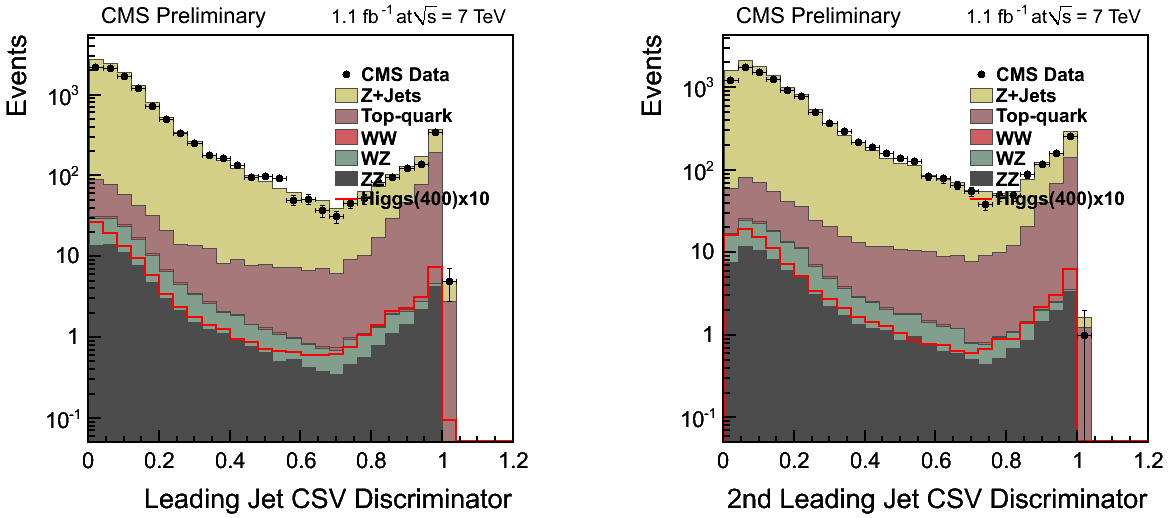

Figure 43: Distribution of the CSV discriminator, leading jet (left) and second leading jet (right) for muon events in 1.1 fb^{-1}.

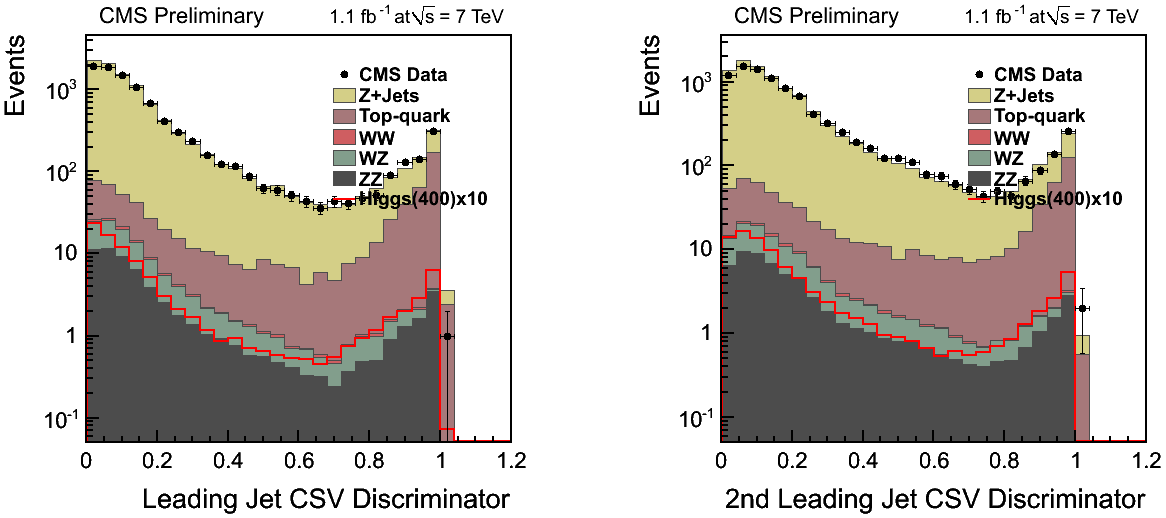

Figure 44: Distribution of the CSV discriminator, leading jet (left) and second leading jet (right) for electron events in 1.1 fb^{-1}.

CMS Preliminary 1.1 fb^{-1}

	Electrons		Muons	
	TCHE	CSV	TCHE	CSV
$t\bar{t}$	28.0	28.5	29.4	29.9
WZ	4.6	6.2	5.6	7.3
WW	0.05	0.02	0.1	0.08
ZZ	6.1	7.6	7.4	9.0
Z+jets	331.6	437.1	384.4	516.6
Total Expected	370.4	479.5	426.8	563.0
Observed	345	440	382	483
Higgs (400)	1.78	1.54	1.99	1.77

Table 24: Number of events in the 1-tag final region using the CSV and the TCHE taggers for 1.1 fb^{-1} of data.

CMS Preliminary 1.1 fb^{-1}

	Electrons		Muons	
	TCHE	CSV	TCHE	CSV
$t\bar{t}$	3.32	3.48	4.04	4.45
WZ	0.14	0.21	0.25	0.33
WW	0	0	0	0.00
ZZ	1.69	2.11	2.24	2.74
Z+jets	20.30	28.69	21.67	32.16
Total Expected	25.45	34.49	28.20	39.69
Observed	30	35	26	38
Higgs (400)	0.65	0.70	0.77	0.79

Table 25: Number of events in the 2-tag final region using the CSV and the TCHE taggers for 1.1 fb^{-1} of data.